Restitic or not? Insights from trace element content and crystal — Structure of spinels in African mantle xenoliths

Davide Lenaz [a,*], Maria Elena Musco [a,b], Maurizio Petrelli [c], Rita Caldeira [d,e], Angelo De Min [a], Andrea Marzoli [f], Joao Mata [e], Diego Perugini [c], Francesco Princivalle [a], Moulay Ahmed Boumehdi [g], Idris Ali Ahmadi Bensaid [g], Nasrrddine Youbi [e,g]

[a] Department of Mathematics and Geosciences, University of Trieste, Trieste, Italy
[b] Istituto Nazionale di Oceanografia e di Geofisica Sperimentale (OGS), Trieste, Italy
[c] Department of Physics and Geology, University of Perugia, Perugia, Italy
[d] Laboratório National de Energia e Geologia (LNEG), Amadora, Portugal
[e] Instituto Dom Luiz, Faculdade de Ciências, Universidade de Lisboa, Lisboa, Portugal
[f] Department of Geosciences, University of Padova, and IGG-CNR, Padua, Italy
[g] Department of Geology, Faculty of Sciences-Semlalia, Cadi Ayyad University, Marrakech, Morocco

ARTICLE INFO

Accepted 16 February 2017

Keywords:
Cr-spinels
Trace elements
Mantle xenoliths
Cameroon
Libya
Morocco

ABSTRACT

The lithospheric architecture of Africa consists of several Archean cratons and smaller cratonic fragments, stitched together and flanked by polycyclic fold belts. Here we investigate the structure and chemistry of spinels from lithospheric mantle xenoliths from distinct tectonic settings, i.e. from the Saharan metacraton in Libya (Waw-En-Namus) which could show archaic chemical features, Cameroon (Barombi Koto and Nyos Lakes) where the Sub Continental Lithospheric Mantle was modified during the Pan-African event and fluxed by asthenospheric melts of the Tertiary Cameroon Volcanic Line and Morocco (Tafraoute, Bou-Ibalrhatene maars) in the Middle Atlas where different metasomatic events have been recorded. From a structural point of view it is to notice that the Libyan spinels can be divided into two groups having different oxygen positional parameter ($u > 0.2632$ and $u < 0.2627$, respectively), while those from Cameroon are in between those values as the Moroccan ones already studied by other authors. The intracrystalline closure temperature (Tc) of the here studied spinels is different among the different samples with one Libyan group (LB I) showing T*c* in the range 490–640 °C and the other 680–950 °C (LB II). Cameroon and Morocco spinels show a T*c* in the range 630–760 °C. About 150 different spinels have been studied for their trace element content and it can be seen that many of them are related to Cr content, while Zn and Co are not and clearly distinguish the occurrences. Differences in the trace element chemistry, in the structural parameters and in the intracrystalline closure temperatures suggest that a different history should be considered for Cameroon, Morocco and LB I and LB II spinels. Even if it was not considered for this purpose, we tentatively used the Fe^{2+}/Fe^{3+} vs. TiO_2 diagram that discriminate between peridotitic and the so-called "magmatic" spinels, i.e. spinel crystallized from melts. LB I and LB II spinels plot in the peridotitic field while Cameroon and Morocco spinels fall in the magmatic one. Consequently, the xenoliths sampled from a probably juvenile SCLM at the edge of the most important lithospheric roots (i.e. Cameroon and Morocco) apparently have spinels possibly fractionated in situ from percolating melts and do not represent a real spinel-peridotite facies. On the contrary mantle xenoliths from Libya exhibit spinels with peridotitic features compatible with a slow ascent of a mantle diapir (plume).

1. Introduction

The lithospheric architecture of Africa consists of several Archean cratons and smaller cratonic fragments, stitched together and flanked by younger polycyclic fold belts. The four larger African cratons (West Africa, Congo, Tanzania and Kaapvaal) are underlain by generally depleted SCLM (Sub Continental Lithospheric Mantle) roots which extend to ≥300 km depth (Begg et al., 2009; O'Reilly et al., 2009). The cratonic margins have repeatedly focused ascending magmas, leading to refertilization and weakening of the SCLM. Less depleted SCLM underlies some polycyclic mobile belts and may have been generated during the Proterozoic (Trompette, 1994), and repeatedly refertilized by uprising magmas during Proterozoic and Phanerozoic tectono-magmatic events.

* Corresponding author.
E-mail address: lenaz@units.it (D. Lenaz).

It is well known that ultramafic xenoliths entrained in mafic alkaline magmas are of great importance because they enable direct investigation of the evolution of compositional and textural evolution within the upper mantle. As a consequence, a lot of crystal chemical studies of their constituent phases have been published. They are mainly focused on clinopyroxenes (Brizi et al., 2003; Cundari et al., 1986; Dal Negro et al., 1984, 1989; Nédli et al., 2009; Princivalle et al., 2000, 2014) and spinels. In particular the studies on spinels from mantle xenolith started in the 1980s (Della Giusta et al., 1986; Princivalle et al., 1989) to reappear in the 3rd millennium (Carraro, 2003; Lenaz et al., 2014a; Nédli et al., 2008; Perinelli et al., 2014; Princivalle et al., 2014; Uchida et al., 2005). The structures and site occupancies of natural and synthetic Cr-bearing spinels have been extensively studied using single-crystal X-ray diffraction techniques (Bosi et al., 2004; Carbonin et al., 1996, 1999; Carraro, 2003; Della Giusta et al., 1986, 1996; Derbyshire et al., 2013; Lenaz et al., 2004, 2011, 2014b, 2014c, 2015; Nédli et al., 2008; Princivalle et al., 1989; Uchida et al., 2005) because of their use as petrogenetic indicators, geobarometers, geothermometers and also for their importance as ore minerals for Cr and platinum group elements.

Here, we study Cr-spinels from mantle xenoliths entrained within Quaternary alkali basalts from Libya and from Cameroon, and will compare them with previously studied samples from Morocco. While the Libya meta-craton was affected by quite sparse Phanerozoic magmatism, Cameroon was the site of almost continuous magmatic activity at least during the Tertiary (Fitton and Dunlop, 1985; Deruelle et al., 2007). Due to such different setting, the SCLM beneath Libya could still retain ancient depleted chemical features not easy to find under the Cameroon Line because of the widespread interaction between magmas of sublithospheric origin with the SCLM as well as its assumed more juvenile nature (Marzoli et al., 2000, 2015). Consequently, the aim of this study is to verify if different chemical, structural and thermometric features are registered in spinels from mantle xenoliths derived from different geodynamic settings as the Saharan metacraton and the Cameroon Volcanic Line. Both occurrences will be, then, compared to spinels from the peri-cratonic SCLM from Morocco recently studied by Lenaz et al. (2014a). The studied Cr-spinels from Tafraoute and Bou-Ibalrhatene maars (Northern Morocco) are enclosed in mantle xenoliths from Plio-Quaternary alkaline basalts characterized by a wide range of lithological and chemical heterogeneity, consistent with variable degree of metasomatism of their lithospheric mantle source (Chanouan et al., in press; El Azzouzi et al., 2010; El Messbahi et al., 2015; Natali et al., 2013; Raffone et al., 2009; Wittig et al., 2010a, 2010b) and testifying ancient melt extraction processes, possibly during Neo- to Paleo-proterozoic times. This scenario is similar to that inferred for other Cenozoic Central-Northern African volcanic centres, such as Hoggar (Algeria; Beccaluva et al., 2007; Kourim et al., 2014) and Gharyan (Libya; Beccaluva et al., 2008; Raffone et al., 2009).

2. Geological setting

The investigated areas, Waw-En-Namus (Libya), Lake Barombi and Lake Nyos (Cameroon), are positioned far from the main African cratons. Libya, and more in general all the north-eastern part of the continent was involved by the Pan-African orogenesis whose structures enclosed the Saharan Metacraton and extend from the Ethiopian rift toward the Western African Craton. The metacraton is bounded by lithospheric-scale suture zones resulting from Neoproterozoic opening-collision events with the surrounding terranes. Abdelsalam et al. (2011) individuates: *i*) to the east, the N-trending Keraf–Kabus–Sekerr Shear Zone separating the Saharan Metacraton from the Arabian–Nubian Shield; *ii*) the N-trending Raghane Shear Zone to the west, which is interpreted as a suture defining the collision zone between the Saharan Metacraton and the Tuareg Shield (Abdelsalam et al., 2011); and *iii*) to the south the E-trending Oubanguides Orogen, which separates the Saharan Metacraton from the Congo Craton (Abdelsalam et al., 2011). This region was marked, from the Late Mesozoic to present (Guiraud, 1998; Lustrino and Wilson, 2007) by intraplate magmatism related to the asthenospheric uplift, which was perhaps responsible of the partial erosion of the Saharan Metacraton lithospheric root.

The Cameroon Volcanic Line is a major feature of the African plate. It is globally N70E oriented, extending from the Gulf of Guinea to Lake Tchad. According to the most accepted structural explanation, the Cameroon Volcanic Line, occurring along a Proterozoic reactivated transtensive fault belt that shows no lithospheric root, represents, at least since Proterozoic times, the suture between the West African and the Congo Cratons. This inter-cratonic region appears as a privileged path for the magma ascent since Proterozoic times as testified by the presence of mainly Devonian and Jurassic basaltic dykes (Tchouankoue et al., 2014) and widespread Cenozoic to recent igneous activity (see review in Nyome and de Wit, 2014). There is little consensus on the cause of the magmatic activity. Among the possible models there are (*i*) the hot spot model; (*ii*) multiple (fingers) plumes; (*iii*) flow from the Afar plume channeled by thinned lithosphere beneath central Africa; (*iv*) decompression melting beneath reactivated shear zones and (*v*) small-scale mantle convection (see review in Nkono et al., 2014). Reusch et al. (2010, 2011) and De Plaen et al. (2014) suggested, based on geophysical data that the sub-lithospheric mantle below Cameroon is characterized by small convective cells, developed between the about 250 km deep roots of the Congo Craton and the relatively shallow (about 100 km thick) Cameroon lithosphere, characterized by a crustal thickness of about 30–35 km. However, Elsheikh et al. (2014) considered that this model could not explain the orientation of the oceanic sector. Based on the existent geophysical data and shear-wave splitting parameters they proposed that the Cameroon Line developed by gradual basal erosion of the underlying lithosphere channeled by the sharp change in the orientation of the western margin of Central Africa (E–W north of the CVL to N–S south of the CVL). Geochemical studies have shown that Cameroon Line magmas were significantly contaminated by (or even issued from) the continental lithospheric mantle and SCLM refertilization events may have occurred at least since the opening of the Equatorial Atlantic (Nyome and de Wit, 2014 and references within). The existence of magma chambers located in the deep crust at 25–30 km depth is suggested by relatively deep, low-energy seismic events (De Plaen et al., 2014) as well as by petrological-mineralogical studies (Marzoli et al., 2015).

The Cenozoic volcanism of the Atlas system (Algeria, Morocco, Tunisia) is exclusively of intraplate alkaline type (alkali basalts, basanites, nephelinites, and associated intermediate and evolved lavas), while in the Rif region it evolved through time from calc-alkaline to shoshonitic and finally alkaline magmas (Duggen et al., 2005, 2009; El Azzouzi et al., 1999, 2010; Maury et al., 2000). It is located within a SW–NE trending volcanic strip, underlain by thinned lithosphere (Frizon De Lamotte et al., 2004; Missenard et al., 2006; Teixell et al., 2005; Zeyen et al., 2005), which crosscuts the major tectonic structures of central Morocco. The Middle Atlas basaltic province comprises the largest and youngest volcanic fields in Morocco. Well-preserved strombolian cones and maars occur along a N–S trend ca.70 km long. K–Ar ages (El Azzouzi et al., 1999, 2010) show that the Middle Atlas volcanic activity occurred during the Miocene, the Pliocene and the Quaternary until 0.6–0.5 Ma. Some maar deposits (Tafraoute, Bou-Ibalrhatene) contain abundant mantle (spinel lherzolites, pyroxenites, garnet-bearing pyroxenites) and crustal xenoliths.

3. Volcanological and petrological observations

3.1. Waw-An-Namus mantle xenoliths (Libya): LB

The age of the volcanism in the Libyan volcanic fields spans from the Paleogene (55–50 Ma) to the Neogene and Quaternary (12–1 Ma;

Permenter and Oppenheimer, 2007). According to Farahat et al. (2006) and Martin and Németh (2006) the magmatism is sodic-alkaline and the rock-types are mainly alkali-basalts, ankaratrites, basanites, trachytes and phonolites. Mantle xenoliths, lherzolitic to harzburgitic in composition, are widespread in the mafic rocks from Gharyan (Beccaluva et al., 2008), Jabal As Sawda (Woller and Fediuk, 1980), Jabal Al Haruj (Németh et al., 2003) and Waw-An-Namus (Bardintzeff et al., 2012; Busrewil and Wadsworth, 1983; Miller et al., 2012).

The Waw-An-Namus volcanic field is dominated by a 4 km wide, 100 m deep caldera containing a post-caldera scoria cone essentially made of phreatomagmatic tephra. Ankaratritic–nephelinitic–basanitic bombs containing peridotite xenoliths are dispersed around the summit crater (Bardintzeff et al., 2012; Busrewil and Wadsworth, 1983).

In this area the mantle xenoliths are represented by spinel lherzolites with medium-coarse granular or protogranular textures. The xenoliths consist of olivine (Fo_{89}–$Fo_{91.8}$), enstatite (Mg# = 90–94), Cr-diopside (Mg# = 94–99.6, Cr_2O_3 = 0.7–1.70 wt.%) and spinel (Cr# = 0.08–0.56; Mg# = 0.69–0.82, $TiO_2 \leq 0.26$ wt.%) , where Mg# and Cr# stands for $Mg/(Mg + Fe^{2+})$ and $Cr/(Cr + Al)$, respectively. Spinels from two different mantle xenoliths are shown in Fig. 1.

3.2. Lake Nyos and Barombi mantle xenoliths (Cameroon): CAM

Lake Nyos and Barombi Koto are maars that belong to the Cameroon Volcanic Line. The last anorogenic igneous events created more than 60 intrusive ring complexes (70–30 Ma; Ngako et al., 2006) and 12 volcanic massifs (51.8 Ma to Present) in the continental segment.

Lake Nyos lies in a phreatomagmatic crater occurring in meta-granitic and granitic Pan-African basement rocks (Dunlop, 1983; Lasserre, 1978) and surrounded by phreatomagmatic breccias. K–Ar determinations point to a Quaternary–Pliocene age ranging between 1.1 and 3.5 Ma (Freeth and Rex, 2000). All eruptive products from different events are basaltic in composition (Temdjim, 2005).

According to Temdjim (2012), the Nyos mantle xenoliths are spinel lherzolites, spinel harzburgites and olivine websterites exhibiting coarse granular or protogranular to weakly porphyroclastic textures. The xenoliths consist of olivine ($Fo_{89.0}$–$Fo_{91.5}$), enstatite (Mg# = 90–92), Cr-diopside (Mg# = 92–98, Cr_2O_3 = 0.7–1.65 wt.%) and Cr-spinel (Mg# = 0.70–0.80; Cr# = 0.097–0.11; $TiO_2 < 0.4$ wt.%) (Pintér et al., 2015; Temdjim, 2012). We sampled only lherzolites.

The Crater Lake Barombi Koto is a lobed sub-circular maar. According to Chako Tchamabé et al. (2013) there were two major volcanic episodes with a complex eruptive evolution, involving variable eruptive styles and fall out deposition, as well as turbulent diluted pyroclastic density currents. Lavas are picrobasalts, basanites, basalts, and hawaiites (Tamen et al., 2007). Mantle xenoliths are, according to Teitchou et al. (2007), lherzolites with protogranular and porphyroclastic textures. Olivine ($Fo_{89.4}$–$Fo_{90.3}$) and orthopyroxene (Mg# = 90–91) display a narrow compositional range. Clinopyroxenes (Mg# = 89–91) have relatively high Cr_2O_3 contents (0.65–1.70 wt.%). Teitchou et al. (2007) found out that spinel Mg# and Cr# vary from 0.74 to 0.78 and from 0.09 to 0.14, respectively.

3.3. Bou-Ibalrhatene and Tafraoute maars (Morocco): MOR

According to Lenaz et al. (2014a), all the investigated mantle xenoliths are lherzolites and harzburgites characterized by a protogranular to granular texture with grain size up to 0.6 mm. Moreover they contain, in particular the harzburgites, minor amounts of interstitial glass always surrounded by reaction rims. Xenoliths are composed by olivine, orthopyroxene, clinopyroxene and rare spinel. Olivine (Fo_{90}) appears quite homogeneous in size (about 400–500 μm), slightly fractured and never altered. Orthopyroxene shows dimensions between 100 and 600 μm and rarely characterized by the presence of clinopyroxene exsolution lamellae. Clinopyroxene (Mg# = 95–98; Cr_2O_3 0.59–1.06 wt.%) ranges between 50 and 400 μm and is often fresh. Spinels are quite uncommon, pale brown in colour and always smaller than 200 μm, idiomorphic and located inside primary olivine or orthopyroxene crystals. Major details can be found in Lenaz et al. (2014a). Spinels from a mantle xenolith are shown in Fig. 1.

4. Experimental procedures

In total, 19 spinels (12 from Libya, 7 from Cameroon) have been analysed by means of X-ray single crystal diffraction and electron microprobe. X-ray diffraction data were recorded on an automated KUMA-KM4 (K-geometry) diffractometer, using MoKα radiation,

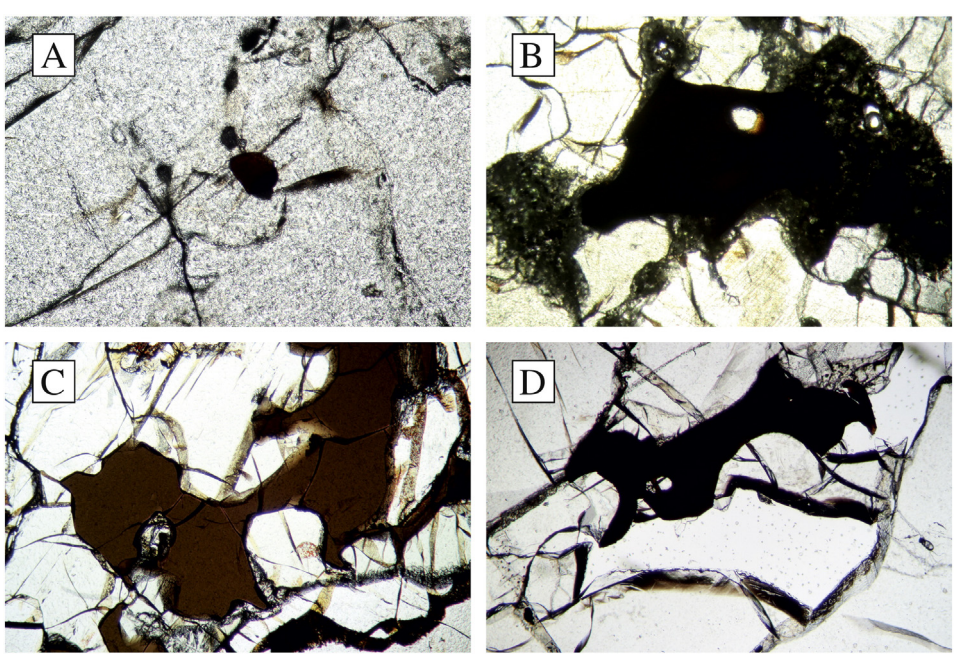

Fig. 1. Spinels from different mantle xenoliths. A: idiomorphic spinel (BI24; Morocco); B: spinels crystallized in a melt pocket (BI24; Morocco); C: non idiomorphic spinel (LB13; Libya); D: non idiomorphic spinel (LB2; Libya).

Table 1
Results of structure refinement a_0: cell parameter (Å); *u*: oxygen positional parameter; T–O and M–O: tetrahedral and octahedral bond lengths (Å), respectively; m.a.n.T and M: mean atomic number; U(M), U(T), U(O): displacement parameters for M site, T site and O; N. Refl.: number of unique reflections; R1 all (%), wR2 (%), GooF as defined in Sheldrick (2008). Diff.peaks: maximum and minimum residual electron density ($\pm$ e/Å^3). Space Group: Fd – 3 m. Origin fixed at −3 m. Z = 8. Reciprocal space range: $-19 \le h \le 19$; $0 \le k \le 19$; $0 \le l \le 19$. Estimated standard deviations in *brackets*. LB I and LB II: Libya; BAR: Barombi (Cameroon); LN: Lake Nyos (Cameroon).

Sample	LB1A	LB1Z	LB3A	LB3B	LB16A	LB16B	LB2A	LB4A	LB6A
	LB I	LB I	LB I	LB I	LB I	LB I	LB II	LB II	LB II
a_0	8.1219 (1)	8.1226 (1)	8.1542 (1)	8.1533 (1)	8.1321 (2)	8.1335 (3)	8.2458 (1)	8.1875 (2)	8.1757 (2)
u	0.26345 (5)	0.26332 (4)	0.26338 (8)	0.26335 (5)	0.26338 (6)	0.26328 (6)	0.2626 (1)	0.2627 (1)	0.2625 (1)
T–O	1.9476 (7)	1.9461 (5)	1.954 (1)	1.9538 (7)	1.9491 (8)	1.9481 (9)	1.965 (1)	1.953 (2)	1.946 (2)
M–O	1.9274 (3)	1.9285 (3)	1.9356 (6)	1.9356 (4)	1.9304 (4)	1.9314 (4)	1.9634 (7)	1.9486 (8)	1.9475 (8)
m.a.n.T	14.90 (8)	14.99 (8)	15.6 (2)	15.3 (1)	14.7 (1)	14.6 (1)	16.6 (3)	16.1 (2)	15.7 (2)
m.a.n.M	14.11 (4)	14.15 (5)	15.8 (2)	15.23 (6)	14.71 (9)	14.76 (6)	19.6 (4)	16.6 (1)	16.2 (1)
U (M)	0.0047 (1)	0.0049 (1)	0.0063 (2)	0.0041 (1)	0.0046 (1)	0.0048 (1)	0.0037 (1)	0.0051 (1)	0.0048 (1)
U (T)	0.0061 (2)	0.0061 (1)	0.0076 (2)	0.0055 (2)	0.0058 (2)	0.0060 (2)	0.0056 (2)	0.0071 (3)	0.0071 (3)
U (O)	0.0063 (1)	0.0067 (1)	0.0078 (2)	0.0061 (1)	0.0061 (1)	0.0064 (1)	0.0062 (3)	0.0088 (2)	0.0088 (3)
N. refl.	162	176	172	184	175	173	170	144	130
R1	2.07	2.16	3.58	2.54	3.02	3.29	2.85	2.72	2.56
wR2	4.98	4.35	7.44	5.78	6.45	6.72	6.29	5.45	4.65
GooF	1.263	1.354	1.251	1.318	1.311	1.379	1.312	1.263	1.249
Diff.peaks	0.45; −0.49	0.47; −0.53	0.85; −1.54	0.72; −0.95	0.62; −1.07	1.02; −1.31	1.55; −2.37	0.72; −1.35	0.63; −1.04

monochromatised by a flat graphite crystal. Data was collected, according to Della Giusta et al. (1996), with up to 55° of 2 θ in the ω–2θ scan mode (scan width 1.8°2θ, counting times from 20 to 50 s, depending on the peak standard deviation). Twenty-four equivalent reflections of (12 8 4), at about 80° of 2θ, respectively, were accurately centred at both sides of 2θ, and the α_1 peak barycentre was used for cell parameter determination. Structural refinement using the SHELX-97 program (Sheldrick, 2008) was carried out against Fo^2_{hkl} in the Fd − 3 m space group (with the origin at −3 m), since no evidence for different symmetry appeared. Scattering factors were taken from Prince (2004) and Tokonami (1965). The crystallographic data are presented in Table 1. Additional Libyan spinels have been analysed by X-ray single crystal diffraction. They appear only in Fig. 2, because after diffraction they have been heated several times at 600 °C for other purposes (Velicogna and Lenaz, 2017) so that original Fe^{2+}/Fe^{3+} may have changed.

Ten to fifteen spot analyses were performed on the same Cr-spinels used for X-ray data collection, using a CAMECA-SX50 electron microprobe (EPMA) at IGG-CNR Padua, operating at 15 kV and 15 nA. A 20 s counting time was used for both peak and total background. Synthetic oxide standards were used. Raw data were reduced by PAP-type correction software provided by CAMECA. The mineral chemical analyses are reported in Table 2.

To have more representative results we analysed by EMPA and Laser Ablation–Inductively Coupled Plasma–Mass Spectrometry (LA-ICP-MS), sixty more spinels from Cameroon and Libya (CAM and LB hereafter, respectively) besides those already analysed by X-ray single crystal diffraction. As one of the goals is to compare the here studied spinels with those of the peri-cratonic Moroccan area already analysed by Lenaz et al. (2014a) by XRD and EMPA, we also added about 40 more chemical analyses (EMPA and LA-ICP-MS) of spinels from Moroccan Tafraoute and Bou-Ibalghatene maars (MOR).

The cation distribution (Table 2) between the T and M sites was obtained with the method described by Carbonin et al. (1996) and Lavina et al. (2002), in which crystal chemical parameters are calculated as a function of the atomic fractions at the two sites and fitted to the observed values. Site atomic fractions were calculated by minimizing the function F(x) (Table 2), which takes into account the mean of the square differences between calculated and observed parameters divided by their squared standard deviations.

A total of 144 (32 LB, 28 CAM and 44 MOR) crystals have been analysed at the Dept. of Physics and Geology, University of Perugia, for trace element determinations. The laser ablation (LA) device was a Teledyne/Photon Machine G2 equipped with a Two-Volume ANU (Australian National University) HelEx 2 cell. The laser source was an ATL-I-LS-R solid-state triggered excimer 193 nm laser. The ablation was performed in Helium (He) atmosphere to enhance the ablation performance, to reduce particles deposition and inter-element fractionation (Eggins et al., 1998; Günther and Heinrich, 1999). Argon (Ar) and Nitrogen (N) were added after the ablation cell to reduce perturbations on the plasma torch and to enhance sensitivity (Hu et al., 2008). The mass spectrometer was a quadrupole based Thermo Scientific iCAP Qc ICP-MS equipped with the high performance interface. LA-ICP-MS operating conditions were optimized before each analytical session by continuous ablation (laser fluence, repetition rate and beam diameter equal to 3.5 J/cm^2, 8 Hz and 85 μm respectively) of NIST SRM 612 glass reference material (Pearce et al., 1997) in order to provide maximum signal intensity (e.g. La > 600,000 cps) and stability (relative standard deviation for La < 2.5%) , while suppressing oxides formation (Th/ThO < 0.5%). Analyses on Cr-spinels have been performed using a laser fluence, repetition rate and beam diameter equal to 3.5 J/cm^2, 8 Hz and 65 μm respectively. The NIST SRM 610 (Pearce et al., 1997) and the USGS BCR2G (Rocholl, 1998) glass reference materials have been used as calibrator (primary standard) and quality control (secondary standard) respectively. The following chemical species have been analysed using Mg as internal standard: Li, Si, Sc, Ti, V, Mn, Co, Ni, Zn, Ga and Cu. Under these operating conditions, precision and accuracy are always better than 10% (please refer to Petrelli et al. 2016 for further details).

5. Results

The unit cell of the spinel structure can be described as a slightly distorted cubic close-packed (ccp) array of 32 oxygen atoms with 8 cations at tetrahedrally coordinated T sites, and 16 cations at octahedrally coordinated M sites (Hill et al., 1979). The T and M sites lie on special positions with −43 m and −3 m symmetry, respectively. The only variable geometrical parameters are the unit-cell edge (a) and oxygen coordinate (u, u, u), which is related to the oxygen packing distortion. The ideal ccp structure shows $u = 0.25$, but it is observed that u is higher than 0.25 for all the Cr-bearing spinels. The observed distortion is a consequence of similar M–O and T–O bond distances ($u = 0.2625$ when distances are equal; Hill et al., 1979).

CAM spinels are very similar among them with cell edges ranging from 8.1268 (1) to 8.1485 (2) Å and oxygen positional parameters, u, within 0.26251 (7) and 0.26278 (9) (Table 1; Fig. 2). On the contrary LB spinels present large variations in both cell edges and u values. This last parameter allowed us to divide the spinels in two subgroups labelled as LB I and LB II. LB I has a limited cell edge variation spanning from 8.1219 (1) to 8.1542 (1) Å and u values between 0.26345 (5) and 0.26328 (6). LB II shows a large cell edge difference, 8.1307 (1)

LB10A	LB10Z	LB14A	BAR	LN05	LN06	LN07	LN08	LN09	LN10
LB II	LB II	LB II							
8.1307 (1)	8.1300 (2)	8.2039 (6)	8.1273 (1)	8.1268 (1)	8.1356 (1)	8.1285 (1)	8.1400 (1)	8.1428 (2)	8.1485 (2)
0.26237 (7)	0.26221 (6)	0.2626 (1)	0.26251 (7)	0.26278 (9)	0.26268 (8)	0.26268 (6)	0.26268 (9)	0.26263 (4)	0.2627 (1)
1.9345 (9)	1.9321 (8)	1.955 (1)	1.936 (1)	1.939 (1)	1.940 (1)	1.9384 (9)	1.941 (1)	1.9410 (6)	1.9434 (7)
1.9374 (5)	1.9383 (4)	1.9533 (8)	1.9355 (5)	1.9334 (6)	1.9362 (6)	1.9346 (5)	1.9373 (6)	1.9384 (3)	1.9392 (3)
15.0 (1)	15.03 (9)	17.3 (3)	14.8 (1)	14.8 (2)	14.8 (1)	14.9 (1)	15.4 (2)	16.27 (8)	15.15 (7)
14.4 (1)	14.44 (5)	17.5 (4)	14.17 (6)	14.2 (2)	14.66 (5)	14.33 (6)	14.6 (1)	15.36 (5)	15.11 (5)
0.0043 (2)	0.0045 (1)	0.0046 (2)	0.0044 (1)	0.0055 (2)	0.0062 (2)	0.0047 (1)	0.0059 (2)	0.0060 (1)	0.0061 (9)
0.0056 (2)	0.0059 (2)	0.0078 (3)	0.0055 (2)	0.0068 (3)	0.0072 (2)	0.0057 (1)	0.0081 (3)	0.0071 (1)	0.0076 (1)
0.0082 (2)	0.0085 (1)	0.0083 (4)	0.0078 (2)	0.0091 (2)	0.0093 (2)	0.0079 (1)	0.0094 (2)	0.0083 (1)	0.00920 (1)
168	183	126	160	181	176	165	168	166	173
2.72	2.56	2.82	2.96	4.18	3.35	2.82	3.51	1.95	2.08
5.57	5.74	4.20	6.73	9.27	7.99	6.34	7.96	3.70	3.38
1.253	1.374	1.222	1.234	1.202	1.232	1.224	1.332	1.292	1.077
0.64; −0.69	0.75; −0.83	0.70; −1.39	0.81; −1.14	1.43; −1.63	0.98; −1.09	0.85; −1.15	1.03; −1.39	0.44; −0.61	0.88; −0.73

to 8.2458 (1) Å, and *u* in the range 0.26237 (7) to 0.2627 (1) (Table 1; Fig. 2).

The chemical analyses performed on the same single crystals used for the structural study reveal that the Cr# is in the range 0.08–0.56 for Libya and 0.09–0.17 for Cameroon samples, while the Mg# varies between 0.69 to 0.81 for Libya and 0.79 to 0.83 for CAM samples (Fig. 3). The different structural spinel groups above defined are also chemically distinct: LB I spinels are characterized by Cr# = 0.07–0.18 and Mg# = 0.76–0.82), LB II by Cr# = 0.12–0.56 and Mg# = 0.69–0.81 while for CAM spinels Cr# and Mg# are in the range 0.08–0.17 and 0.79–0.84, respectively. As far as concerns the minor oxides in LB samples, TiO_2 is usually below 0.15 wt.%, MnO below 0.25 wt.%, NiO between 0.1 and 0.4 wt.%. In CAM, TiO_2 is on average higher than in the LB samples but lower than 0.2 wt.%, except for LN09 approaching 0.5 wt.% TiO_2. The MOR spinels show Cr# in the range 0.10–0.35 and Mg# between 0.34 and 0.82.

When considering the cation distribution, the inversion degree (trivalent cations in T site), *i*, is in the range 0.07–0.21 for LB, and 0.15–0.21 for CAM crystals. By using the geothermometer of Princivalle et al. (1999) it was possible to calculate the intracrystalline closure temperature (T*c*) derived from the Mg–Al exchange between the two sites M and T. The spinels of the LB I group with high *u* (higher than 0.2630) show values in the range 480–640 °C, while those with lower *u* values (lower than 0.2627) are in the range 680–950 °C. CAM samples show a more limited range between 630 and 760 °C.

Among the minor elements, Ni is the most abundant. Its content is in the range 1148–3862 ppm in LB samples, 2950–3920 in CAM, and 2238–3922 ppm in MOR. It is followed by Mn (760–1458 LB; 761–970 CAM; 824–1217 MOR), Zn (742–1580 LB; 414–771 CAM; 463–966 MOR), V (404–1116 LB; 377–519 CAM; 407–907 MOR) and Co (271–372 LB; 202–267 CAM; 229–281 MOR). Gallium (38–89 LB; 65–150 CAM; 65–95 MOR), Cu (1.88–8.13 LB; 1.48–4.91 CAM;

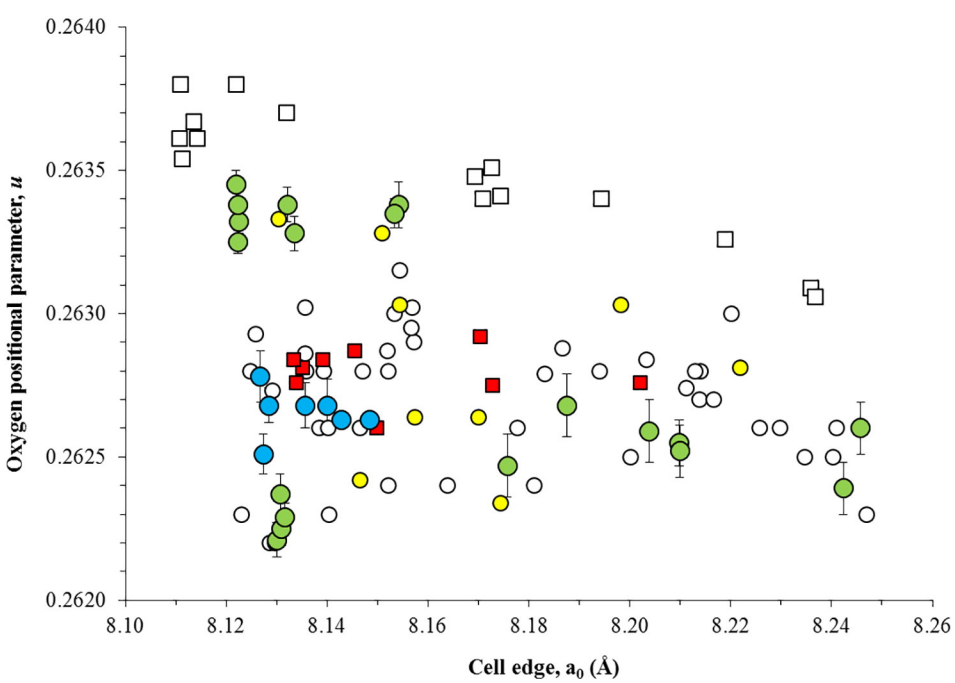

Fig. 2. Oxygen positional parameter, *u*, vs. cell edge, *a*. Green circle: Libya spinels (this study); blue circle: Cameroon (this study); red square: Morocco (Lenaz et al., 2014a); yellow circle: Antarctica (Perinelli et al., 2014); open circle: mantle xenoliths worldwide (Carraro, 2003; Della Giusta et al., 1986; Nédli et al., 2008; Princivalle et al., 1989, 2014; Uchida et al., 2005); open square: Balmuccia and Ronda peridotite massifs (Basso et al., 1984; Lenaz et al., 2010). (For interpretation of the references to color in this figure legend, the reader is referred to the web version of this article.)

Table 2
Chemical analyses and cation distribution. Mean chemical analyses (10–25 spot analyses for each crystal) and cation distribution in T and M site of the analysed Cr-spinels on the basis of four oxygen atoms per formula unit. Fe^{3+} from stoichiometry. F(x): minimization factor which takes into account the mean of square differences between calculated and observed parameters, divided by their standard deviations. Estimated standard deviations are in brackets. Intracrystalline closure temperature calculated by using the thermometer by Princivalle et al. (1999). Cr#: Cr/(Cr + Al); Mg#: Mg/(Mg + Fe^{2+}); Fe#: Fe^{3+}/(Fe^{3+}+Al + Cr).

Sample	LB1A	LB1Z	LB3A	LB3B	LB16A	LB16B	LB2A	LB4A	LB6A	LB10A	LB10Z	LB14A	BAR	LN05	LN06	LN07	LN08	LN09	LN10
MgO	20.9 (1)	21.1 (2)	19.2 (2)	18.9 (1)	20.7 (2)	20.2 (3)	15.3 (1)	17.8 (2)	18.6 (2)	20.7 (1)	20.9 (2)	16.0 (2)	21.5 (1)	21.7 (1)	20.9 (2)	21.0 (1)	21.1 (1)	20.4 (1)	20.6 (1)
Al_2O_3	60.1 (2)	59.3 (4)	50.2 (4)	50.2 (2)	56.3 (2)	55.5 (3)	24.3 (1)	40.6 (2)	43.5 (2)	57.1 (2)	56.4 (6)	33.8 (4)	56.7 (2)	58.6 (2)	55.7 (1)	58.3 (2)	54.7 (3)	54.9 (3)	52.1 (2)
TiO_2	0.12 (2)	0.12 (2)	0.07 (2)	0.07 (1)	0.11 (2)	0.12 (3)	0.11 (2)	0.10 (2)	0.04 (1)	0.05 (2)	0.05 (2)	0.05 (2)	0.16 (2)	0.14 (1)	0.11 (1)	0.10 (2)	0.13 (3)	0.52 (2)	0.05 (1)
Cr_2O_3	7.51 (9)	7.6 (1)	17.4 (1)	17.4 (3)	12.4 (3)	13.1 (2)	45.3 (4)	28.5 (1)	26.2 (3)	11.2 (2)	11.4 (1)	33.5 (3)	8.6 (2)	8.4 (2)	12.4 (2)	8.94 (8)	12.5 (3)	10.0 (2)	15.9 (2)
MnO	0.10 (2)	0.10 (2)	0.12 (3)	0.12 (2)	0.10 (3)	0.12 (3)	0.20 (3)	0.16 (2)	0.15 (2)	0.12 (2)	0.10 (2)	0.19 (2)	0.10 (3)	0.10 (2)	0.11 (2)	0.11 (2)	0.10 (3)	0.10 (2)	0.11 (3)
FeO_{tot}	10.7 (1)	10.8 (2)	13.1 (1)	13.3 (2)	10.6 (1)	10.3 (3)	14.6 (1)	11.2 (2)	11.7 (1)	10.5 (1)	10.6 (2)	16.5 (2)	10.63 (1)	11.2 (1)	10.45 (8)	11.3 (1)	11.75 (9)	14.0 (2)	11.7 (2)
NiO	0.42 (3)	0.41 (3)	0.31 (2)	0.32 (3)	0.36 (4)	0.33 (2)	0.13 (3)	0.22 (4)	0.22 (4)	0.36 (4)	0.37 (4)	0.17 (2)	0.40 (5)	0.42 (4)	0.35 (3)	0.40 (4)	0.39 (3)	0.41 (4)	0.35 (5)
Sum	99.80	99.48	100.42	100.27	100.51	99.7	99.87	100.82	100.31	100.02	99.78	100.047	100.03	100.49	100.01	100.08	100.65	100.36	100.76
FeO	9.2 (1)	8.5 (2)	10.4 (1)	10.9 (2)	9.1 (1)	9.4 (3)	12.3 (1)	11.2 (2)	10.3 (1)	8.9 (1)	8.6 (2)	12.7 (2)	8.1 (1)	8.0 (1)	8.48 (8)	8.8 (1)	8.38 (9)	9.6 (2)	8.7 (2)
Fe_2O_3	1.7	2.5	3.0	2.7	1.7	1.0	2.5	2.5	1.6	1.8	2.2	4.1	2.7	3.5	2.19	2.7	3.75	4.9	3.32
Sum	99.97	99.73	100.72	100.54	100.68	99.81	100.12	101.07	100.47	100.20	100.00	100.49	100.30	100.84	100.23	100.35	101.03	100.85	101.09
T site																			
Mg	0.698 (3)	0.693 (7)	0.734 (7)	0.695 (4)	0.717 (5)	0.707 (9)	0.673 (5)	0.640 (4)	0.616 (5)	0.613 (3)	0.657 (7)	0.549 (6)	0.668 (4)	0.669 (4)	0.669 (4)	0.665 (4)	0.672 (4)	0.645 (4)	0.670 (3)
Al	0.1061 (9)	0.107 (2)	0.052 (1)	0.067 (1)	0.100 (1)	0.111 (2)	0.0207 (7)	0.085 (1)	0.128 (2)	0.185 (2)	0.197 (3)	0.081 (2)	0.149 (1)	0.125 (1)	0.142 (1)	0.141 (1)	0.100 (1)	0.117 (2)	0.115 (1)
Mn	0.0022 (4)	0.0022 (4)	0.0029 (7)	0.0027 (5)	0.0022 (7)	0.0027 (7)	0.0051 (8)	0.0037 (5)	0.0035 (5)	0.0026 (4)	0.0022 (4)	0.0046 (5)	0.0021 (7)	0.0022 (4)	0.0024 (4)	0.0024 (4)	0.0021 (7)	0.0022 (4)	0.0024 (7)
Fe^{2+}	0.161 (3)	0.149 (4)	0.148 (2)	0.181 (3)	0.156 (3)	0.160 (6)	0.245 (3)	0.218 (3)	0.220 (2)	0.172 (2)	0.136 (4)	0.300 (4)	0.127 (2)	0.106 (2)	0.1445 (2)	0.138 (2)	0.151 (2)	0.150 (3)	0.148 (3)
Fe^{3+}	0.033 (3)	0.049 (6)	0.064 (6)	0.054 (5)	0.024 (4)	0.019 (8)	0.057 (5)	0.053 (5)	0.033 (5)	0.027 (3)	0.007 (3)	0.065 (6)	0.054 (4)	0.073 (4)	0.042 (4)	0.053 (4)	0.073 (4)	0.087 (4)	0.065 (4)
M site																			
Mg	0.096 (1)	0.111 (3)	0.022 (1)	0.052 (1)	0.076 (2)	0.079 (3)	0.0095 (5)	0.094 (2)	0.142 (2)	0.185 (2)	0.145 (3)	0.133 (3)	0.152 (2)	0.128 (2)	0.139 (2)	0.136 (2)	0.138 (2)	0.147 (2)	0.130 (1)
Al	1.706 (4)	1.685 (7)	1.521 (7)	1.512 (5)	1.613 (5)	1.598 (9)	0.840 (4)	1.235 (5)	1.273 (6)	1.551 (4)	1.523 (9)	1.070 (9)	1.619 (5)	1.631 (4)	1.558 (5)	1.621 (4)	1.566 (5)	1.563 (6)	1.490 (4)
Ti	0.0023 (4)	0.0023 (4)	0.0014 (4)	0.0014 (2)	0.0021 (4)	0.0024 (6)	0.0025 (5)	0.0021 (4)	0.0008 (2)	0.0010 (4)	0.0010 (4)	0.0011 (4)	0.0031 (4)	0.0027 (2)	0.0021 (2)	0.0019 (4)	0.0025 (6)	0.0102 (4)	0.0010 (2)
Cr	0.152 (2)	0.155 (2)	0.364 (3)	0.366 (5)	0.252 (5)	0.270 (5)	1.077 (7)	0.622 (3)	0.565 (6)	0.228 (3)	0.234 (3)	0.762 (6)	0.172 (2)	0.167 (4)	0.254 (5)	0.181 (2)	0.256 (5)	0.205 (4)	0.328 (4)
Fe^{2+}	0.035 (1)	0.036 (2)	0.083 (2)	0.061 (2)	0.039 (1)	0.043 (3)	0.064 (2)	0.041 (1)	0.0149 (6)	0.0205 (8)	0.049 (2)	0.0050 (5)	0.046 (1)	0.062 (2)	0.0390 (8)	0.052 (1)	0.0297 (8)	0.058 (2)	0.043 (2)
Fe^{3+}	0.0001 (1)	0.0010 (9)	0.0003 (4)	0.006 (5)	0.010 (3)	0.0001 (5)	0.0023 (9)	0.0001 (2)	0.000	0.007 (2)	0.035 (6)	0.024 (3)	0.0001 (1)	0.0001 (1)	0.0006 (5)	0.0007 (4)	0.0002 (2)	0.008 (1)	0.003 (3)
Ni	0.0086 (6)	0.0085 (6)	0.0066 (4)	0.0069 (6)	0.0077 (8)	0.0069 (4)	0.0031 (7)	0.0049 (9)	0.0048 89)	0.0075 (8)	0.0077 (8)	0.0039 (5)	0.008 (1)	0.0078 (8)	0.0073 (6)	0.0080 (8)	0.0082 (6)	0.0086 (8)	0.008 (1)
Cr#	0.08	0.08	0.19	0.19	0.13	0.14	0.56	0.32	0.29	0.12	0.12	0.40	0.09	0.09	0.13	0.09	0.13	0.11	0.17
Mg#	0.80	0.81	0.77	0.76	0.80	0.80	0.69	0.74	0.76	0.81	0.81	0.69	0.83	0.83	0.82	0.81	0.82	0.79	0.81
Fe#	0.02	0.03	0.03	0.03	0.02	0.01	0.03	0.03	0.02	0.02	0.02	0.04	0.03	0.04	0.02	0.03	0.04	0.05	0.03
F(X)	0.155	0.312	0.372	0.178	0.336	0.177	0.253	0.083	0.007	0.012	0.16	0.034	0.297	0.633	0.017	0.118	0.672	0.635	0.048
T°C	573	585	485	557	595	641	676	794	937	914	943	930	743	659	764	726	630	698	721

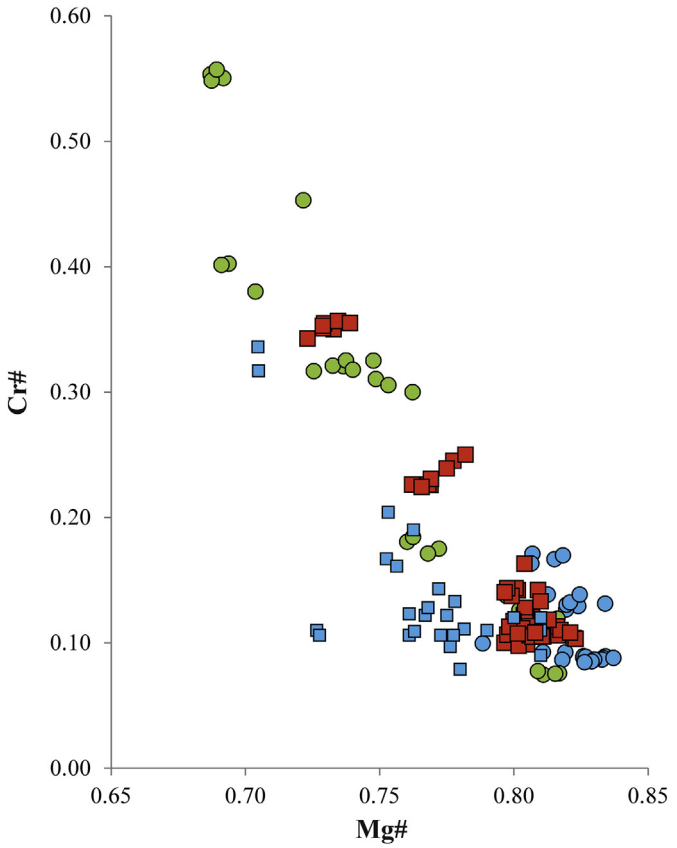

Fig. 3. Cr# vs. Mg#. Green circle: Libya spinels (this study); blue circle: Cameroon; red square: Morocco; blue squares: spinels from Barombi, Lake Nyos and Ngaoundéré by Temdjim (2012), Pintér et al. (2015) and Nkouandou et al. (2015). (For interpretation of the references to color in this figure legend, the reader is referred to the web version of this article.)

0.48–8.08 MOR) and Sc (0.08–2.67 LB; 0.32–1.39 CAM; 0.22–1.66 MOR) are the less abundant. It is to notice that for certain elements CAM and MOR show similar behaviour and that there is no or poor overlapping between them and the LB spinels. These elements are Zn where all the LB spinels are higher than 742 ppm and few CAM and MOR spinels exceed this value, and Co that is higher than 271 in LB spinels with only few spinels from MOR reaching this value. When considering the other elements two different behaviours can be recognized with LB II spinels differing from the others. When considering Sc, V and Mn, LB II spinels differ from the other structural groups. In fact, LB II spinels have higher concentrations of Sc, V and Mn, but low contents of Ni and Ga as compared with the other 3 groups (LB I, CAM and MOR) which, for these elements present identical compositions.

When comparing the content of Cr_2O_3 with the minor elements it is possible to recognize a positive correlation with V and Mn and a negative one with Ni and, at a lesser degree, Ga (Fig. 4).

6. Discussion and conclusions

Large variations in trivalent cations, especially Cr, have been commonly considered the main responsible of changes in the cell edges of Cr-spinels and chromites from layered mafic complexes (Lenaz et al., 2007, 2011, 2012), ophiolites (Derbyshire et al., 2013; Lenaz et al., 2014b, 2014c), komatiites (Lenaz et al., 2004), as well as kimberlites and diamond inclusions (Lenaz et al., 2009). More precisely, for those cases the changes are related to the Cr + Fe^{3+} content. In the mantle xenolith spinels, where the Fe^{3+} content is very low, the cell edge could be directly related to the Cr# showing an R^2 value close to 0.96 (Fig. 5; Carraro, 2003; Della Giusta et al., 1986; Lenaz et al., 2014a, 2014b, 2014c; Nédli et al., 2008; Perinelli et al., 2014; Princivalle et al., 1989, 2014; Uchida et al., 2005). Due to the fact that in each mantle xenolith suite there is a characteristic *u* value for all the spinels, independently from their chemistry, Princivalle et al. (1989) related the *u* values of the mantle xenolith spinels to their cooling history and even with the closure temperature (T*c*), i.e. the temperature at which the intracrystalline exchange reaction practically stopped (Lucchesi et al., 2010). This *u* value is 0.2628 (1) for Morocco samples (Lenaz et al., 2014a), 0.2624 (1) for Mt. Leura, 0.2625 (1) for NE Brazil and Mt. Noorat, 0.2627 (1) for Assab (Princivalle et al., 1989), 0.2628 (1) for Predazzo (Carraro, 2003) and 0.2629 (1) for San Carlos (Arizona; Uchida et al., 2005) (Fig. 2). According to Lucchesi et al. (2010), for spinels in mantle xenoliths the cooling events should be related to the cooling rate of the lava hosting the xenoliths, to the size of the xenoliths and to the position of the crystal within the xenoliths. This is because it is expected that large xenoliths will cool more slowly than small ones and crystals close to the rim will close at a higher temperature than those located in the core of the xenolith. Lenaz et al. (2010) on the basis of the existent literature data reported that the T*c* of spinels from mantle xenoliths was in the range 700–1000 °C, while Lenaz et al. (2014a) extended T*c* to lower values finding, for Morocco spinels, T*c* in the range 560–750 °C. For this last case, these authors suggested that the T*c* could be related to a possible shallow depth of equilibration (about 20–40 km; close to the Moho discontinuity) and not to the temperature of the host lava, similarly to what happened to the Ronda alpine peridotite (Lenaz et al., 2010). Perinelli et al. (2014) described spinels from two localities 80 km apart in Northern Victoria Land (Antarctica) with two very distinctive oxygen positional parameter values. For the BR spinels, *u* is in the range 0.2623–0.2626 while for the GR spinels it varies from 0.2628 to 0.2633, leading to very different intracrystalline closure temperatures of 880–910 and 590–670 °C, respectively. Considering that the mantle xenoliths were probably disrupted at the same depth within the mantle by an uprising magma, Perinelli et al. (2014) argued that even for mantle xenoliths there could be a chemical control on the oxygen positional parameter, suggesting that different *u* values are caused by the higher Fe^{3+} content and cation vacancies present in the GR spinels due to the existence relation among these values. Perinelli et al. (2014) considered powder Mössbauer analyses combined with single crystal X-ray diffraction a valuable method to determine the real amount of Fe^{3+} and cation vacancies as previously reported also by Bosi et al. (2004) and Lenaz et al. (2004). However, Lenaz et al. (2013, 2014b) pointed out that powder Mössbauer can yield significant errors given the fact that, within a powder, there could be grains of spinels which suffered different oxidation degrees causing large differences in the calculated $Fe^{3+}/\Sigma Fe$ ratios that could be avoided by using a point-Mössbauer source.

In this study, we report a situation in which mantle xenoliths (LB samples) erupted from the same volcano have distinctive spinel *u* and T*c* values. There are no significant differences in the occurrence of the mantle xenoliths, their size is similar as is the composition of their hosting lava, the position of the sampled crystal is in the core. Therefore, all the points summarized by Lucchesi et al. (2010) would point to similarities in both *u* and T*c* values. Moreover, they occur in bombs so that the supposed *u* values should be quite low due to the very fast cooling history of those spinels and of their host lavas.

The small size of the here-studied crystals and the low total iron does not allow determining the $Fe^{3+}/\Sigma Fe$ ratio via a point-Mössbauer source. Anyway, considering the Fe^{3+} calculated according to the stoichiometry of these spinels, and not having evidence of possible cation vacancies, it is possible to see in Fig. 6 that even if it seems that there is a correlation between the intracrystalline closure temperature and the Fe^{3+} content for the Libyan samples, this is not present for all the other crystals here studied as well for other spinels from the literature. As it can be seen in Fig. 6, CAM spinels show T*c* in a limited range 630–760 °C that is, more or less intermediate between those of LB I and LB II, and similar to that of Morocco samples.

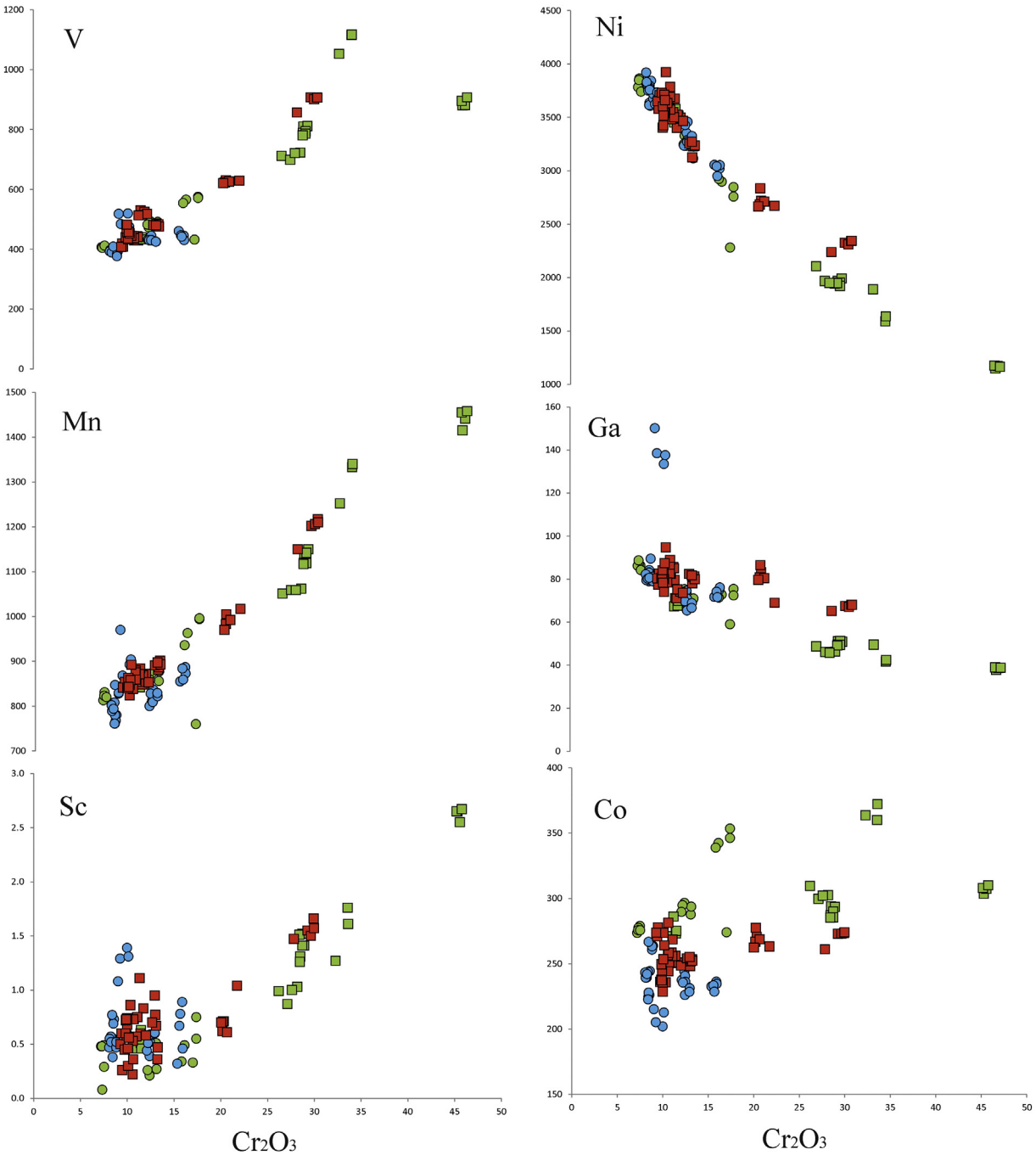

Fig. 4. V, Mn, Sc, Ni, Ga and Co (ppm) vs. Cr_2O_3 (wt.%). Symbols as in Fig. 2.

Differences in the trace element chemistry, in the structural parameters and in the intracrystalline closure temperatures suggest that a different history should be considered for CAM, MOR, LB I and LB II spinels. Even if it was not considered for this purpose, we tentatively used the Lenaz et al. (2000) and Kamenetsky et al. (2001) Fe^{2+}/Fe^{3+} vs. TiO_2 diagram. According to those authors this diagram should discriminate between peridotitic and the so-called "magmatic" spinels, i.e. spinel crystallized from melts (Fig. 7). Therefore, Fe^{2+}/Fe^{3+} vs. TiO_2 variations should be helpful in discriminating restitic spinels from those crystallized from melts. LB I and LB II spinels plot in the peridotitic field while CAM spinels fall almost all in the magmatic field, with the only exception of spinels from the nodule LN06. Spinels from LN10 fall in between the two fields. MOR spinels too fall in the magmatic field.

If we consider all previously published Tc for spinels and their magmatic or peridotitic affinity, it is possible to divide the magmatic spinels into two groups (Fig. 8). One group yields *Tc* in the range 550 to 770 °C and the other group shows a narrower range between 730 and 880 °C. In our opinion, these values could be related to the different temperatures of the intruding melts and the cooling rates of the spinel themselves equilibrating at a certain depth in the mantle. On the contrary the peridotitic spinels show a wide spread of Tc from 480 to about 1200 °C. It seems unlikely that this large range of temperatures could be related to the explanations given by Princivalle et al. (1989) and Lucchesi et al. (2010) or even to the Fe^{3+} content as suggested by Perinelli et al. (2014). Instead, we propose that the low *u*–high Tc LB II group spinels recorded a deep origin, possibly at the spinel to garnet peridotite boundary and have been brought quickly to the surface from there without stalling at

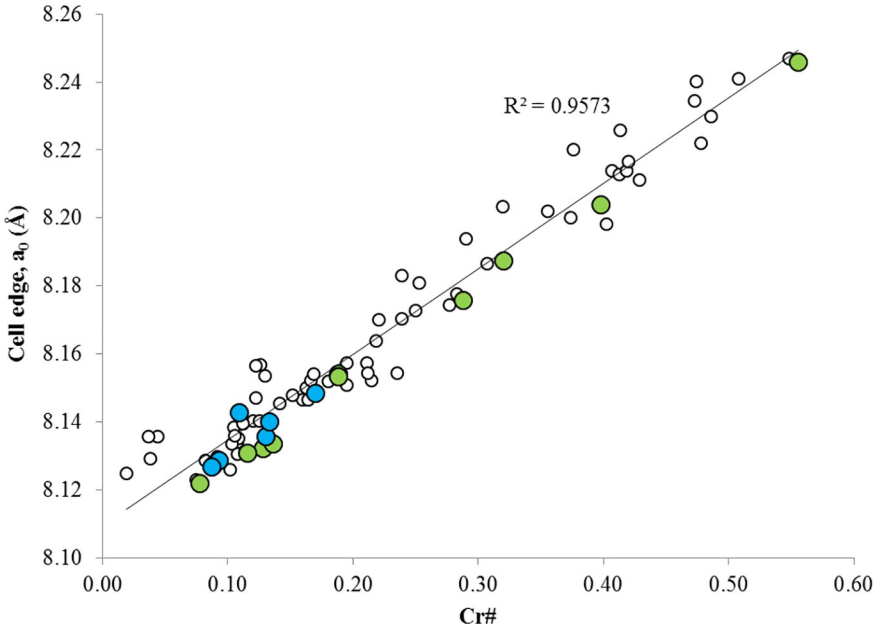

Fig. 5. Cell edge, a, vs. Cr#. Green circle: LB spinels; blue circle: CAM; open circle: mantle xenoliths worldwide (Carraro, 2003; Della Giusta et al., 1986; Lenaz et al., 2014a; Nédli et al., 2008; Perinelli et al., 2014; Princivalle et al., 1989, 2014; Uchida et al., 2005). (For interpretation of the references to color in this figure legend, the reader is referred to the web version of this article.)

intermediate depths. A confirmation of this can be found in Bardintzeff et al. (2012) who suggested, based on petrographic evidence, that the volcanism in the Libyan volcanic field is due to low-degree partial melting of a garnet- and amphibole-bearing mantle source at a depth of 80–100 km. On the contrary, the high *u*–low T*c* LB I spinels probably had a different depth story. Their similarity with the Morocco samples, in fact, suggests that they possibly equilibrated at a shallow depth, about 30 km. In any case, the here-studied spinels seem to be part of the primary peridotite group, being peridotitic and not magmatic, even if different authors found out evidences of metasomatism in these mantle xenoliths (Bardintzeff et al., 2012; Beccaluva et al., 2008).

The distributions of minor- and trace elements in chromite recently provided new insights into the genesis and/or successive evolution (metamorphism) of the chromitites in ophiolitic rocks (e.g., Akmaz

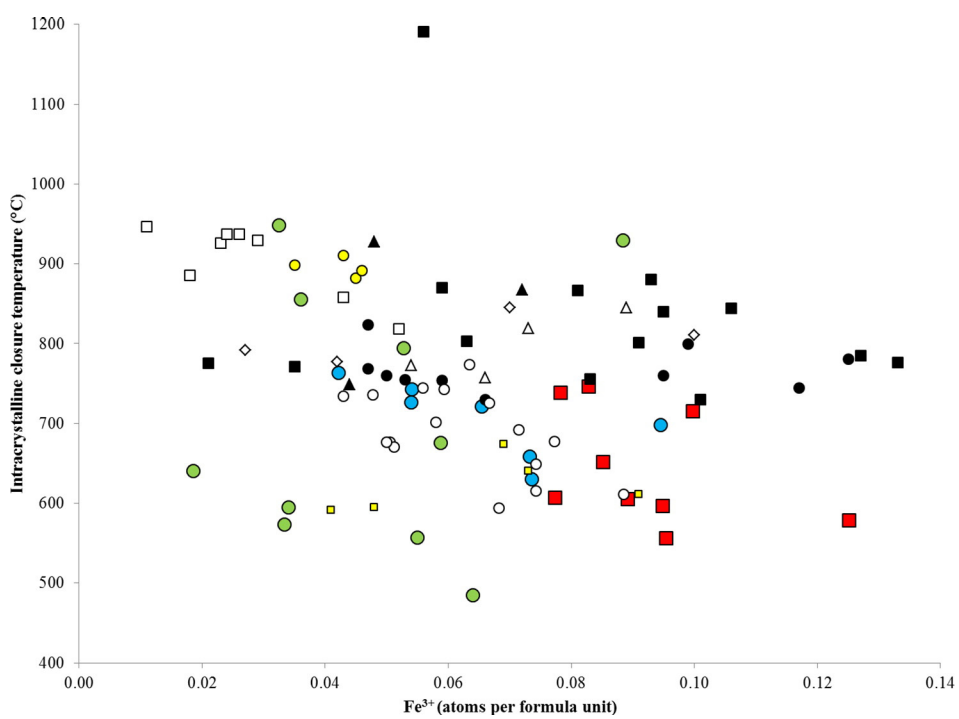

Fig. 6. Intracrystalline closure temperature vs. Fe^{3+}_{tot}. Green circle: Libya spinels (this study); blue square: Cameroon (this study); red square: Morocco (Lenaz et al., 2014a); yellow circle: BR spinels (Antarctica; Perinelli et al., 2014); yellow square: GP spinels (Antarctica; Perinelli et al., 2014); open square: Mt. Leura (Della Giusta et al., 1986); open diamond: NE Brazil (Princivalle et al., 1989); open triangle: Assab (Princivalle et al., 1989); full triangle: Mt. Noorat (Princivalle et al., 1989); full circle: Predazzo (Carraro, 2003); open circle: Hannuoba (China; Princivalle et al., 2014); full square: San Carlos (Arizona; Uchida et al., 2005). (For interpretation of the references to color in this figure legend, the reader is referred to the web version of this article.)

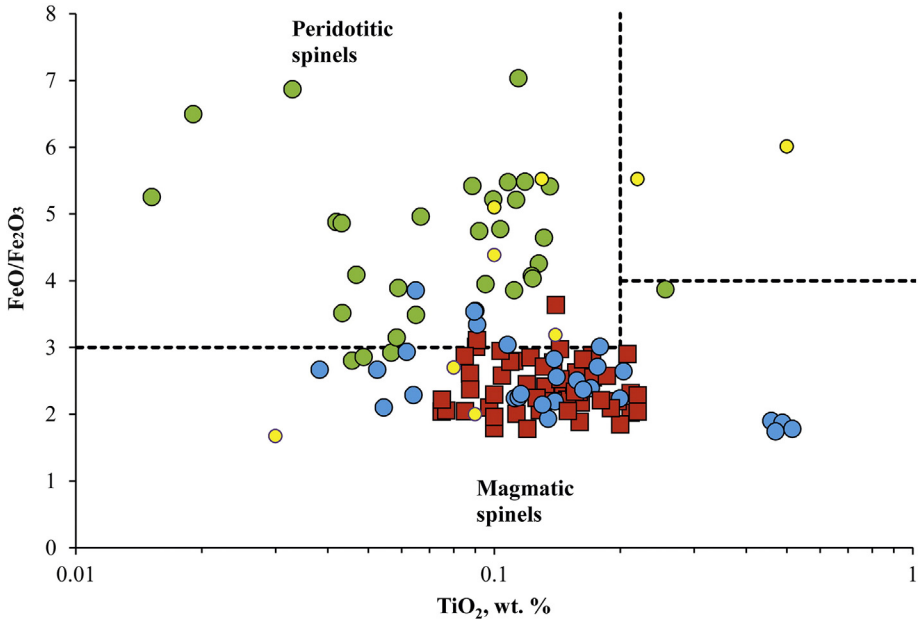

Fig. 7. FeO/Fe_2O_3 vs. TiO_2. Peridotitic and magmatic field of spinels according to Lenaz et al. (2000) and Kamenetsky et al. (2001). Green circle: Libya spinels (this study); blue circle: Cameroon (this study); red square: Morocco; yellow circle: Antarctica (Perinelli et al., 2014). (For interpretation of the references to color in this figure legend, the reader is referred to the web version of this article.)

et al., 2014; Colás et al., 2014; Dare et al., 2009; González-Jiménez et al., 2011, 2014, 2015; McGowan et al., 2015; Pagé and Barnes, 2009; Zhou et al., 2014). According to these authors, the use of the chromite trace-element data (especially Ga, Ni, Zn, Co, Mn, V and Sc), in combination with major-element data provides a better understanding of the geochemistry of these mantle rocks. Literature dealing with minor and trace element distributions in Cr-spinels from other occurrences are very limited. To our knowledge in this field we should consider one recent study by Di Rocco et al. (2012) discussing spinels in endoskarns, where only V (58–66 ppm), Co (11–4 ppm), Ni (2–49 ppm) and Zn (600–1000 ppm) are present in amounts >1 ppm and a couple of analyses of spinels included in garnet from the Zagadochnaya kimberlite (Ziberna et al., 2013). As far as concern mantle xenoliths, Raffone et al. (2009) analysed only Sc, V and REE. No analyses of Ga, Zn, Co are present. In such a view it is difficult to compare our samples with literature data, anyway, it is evident that, apart, from those elements that are related to Cr_2O_3 content, other elements allow to discriminate between the so-called peridotitic spinels and those crystallized from magma, i.e. Zn and Co where peridotitic and "magmatic" spinels fall in two different groups (Fig. 9).

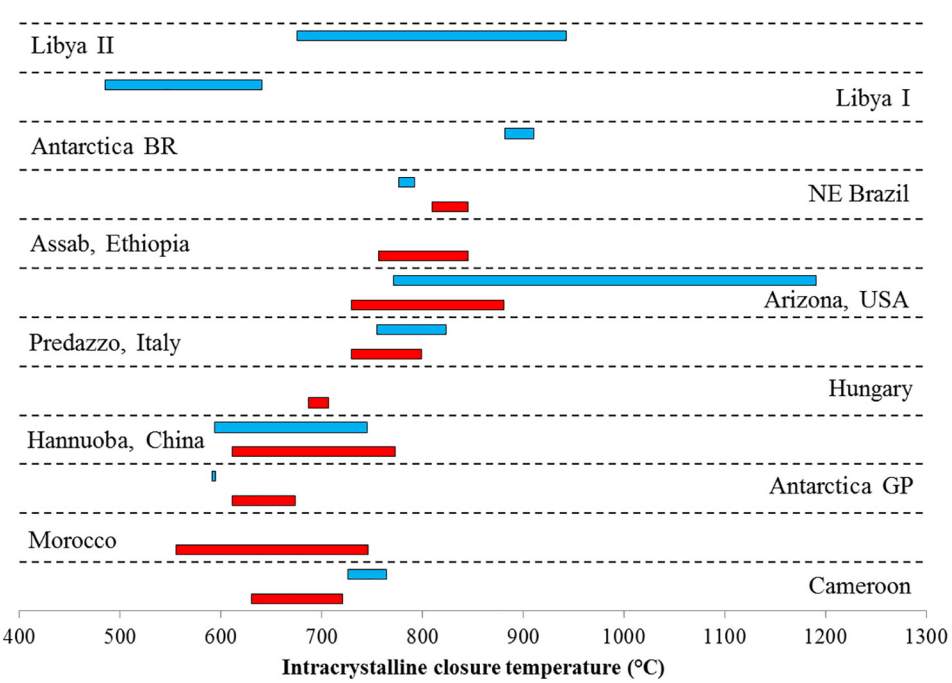

Fig. 8. Range of intracrystalline closure temperatures for the studied spinels and mantle xenoliths used for comparison (Mt. Leura, Della Giusta et al., 1986; Mt. Noorat, NE Brazil, Assab, Princivalle et al., 1989; San Carlos, Uchida et al., 2005; Predazzo, Carraro, 2003; Morocco, Lenaz et al., 2014a; Antarctica, Perinelli et al., 2014; Hannuoba, Princivalle et al., 2014). Red bar: magmatic spinels; blue bar: peridotitic spinels. (For interpretation of the references to color in this figure legend, the reader is referred to the web version of this article.)

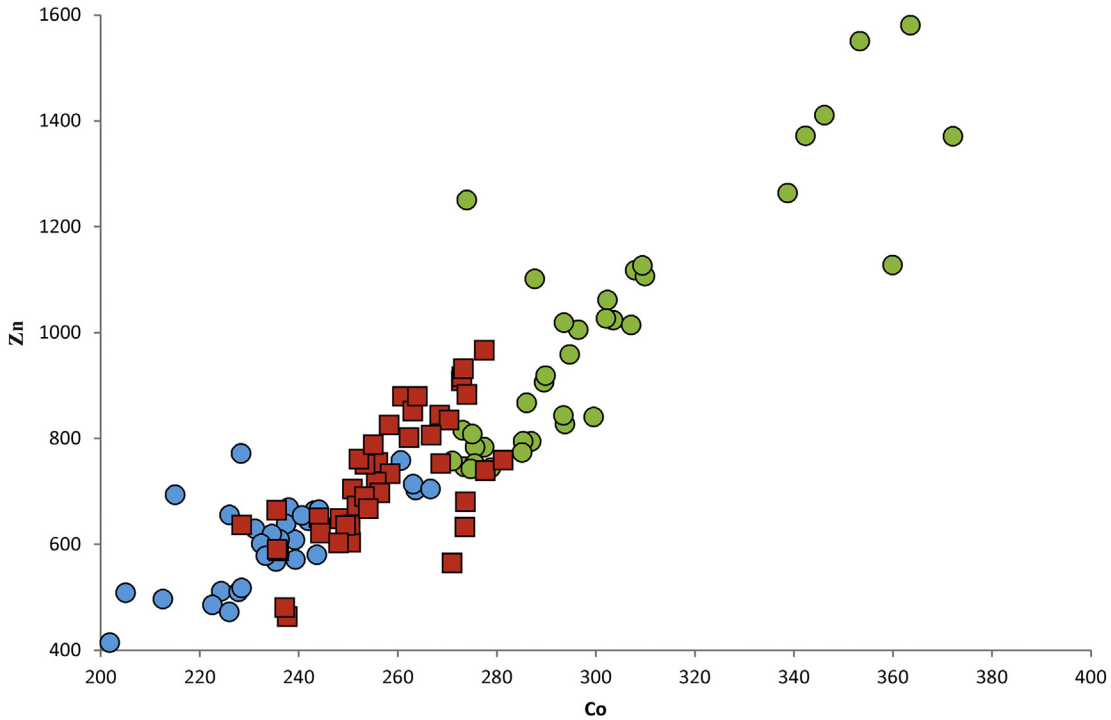

Fig. 9. Zn (ppm) vs. Co (ppm). Symbols as in Fig. 2.

Based on petrographic observations and chemical-mineralogical and geothermobarometric data on Lake Nyos xenoliths, Temdjim (2012) pointed out to an upper mantle uplift beneath the Cameroon Volcanic Line possibly induced by the heating of the lithospheric mantle by the emplacement of a deep mantle plume. The features described by Temdjim (2012) suggested that a couple of their xenoliths initially equilibrated at deeper depth (>60 km) followed by a decompression linked to diapirism of the astenospheric mantle and followed by the final equilibration at a depth of about 30 km. Moreover, Princivalle et al. (2000) suggested that the protogranular texture of the Lake Nji mantle xenoliths testifies that the spinel peridotite and the associated small-volume melts completely re-equilibrated at the spinel-peridotite facies.

Among the here-studied CAM samples we did not find evidence of the deeper mantle xenoliths, while all the other xenoliths show features resembling a situation of final equilibration at about 30 km depth. The associated spinels with their low T*c* and *u* values similar to those of the Moroccan spinels (Lenaz et al., 2014a) suggest a depth in the range 20–40 km, consistent with the results of Temdjim (2012). El Messbahi et al. (2015) found out for the Morocco maars also considered by Lenaz et al. (2014a) that the Bou Ibalghatene mantle was densely fluxed by high melt fractions, mostly focused in melt conduits, while the Tafraoute suite records heterogeneous infiltration of smaller melt fractions that migrated diffusively, by intergranular porous flow.

In summary, the xenoliths sampled from a probably juvenile SCLM at the edge of the most important lithospheric roots (i.e. Morocco and Cameroon) apparently have spinels possibly fractionated in situ from percolating melts and probably do not represent a real spinel-peridotite facies. On the contrary mantle xenoliths from Libya exhibit spinels with peridotitic features compatible with a slow ascent of a mantle diapir (plume).

We also demonstrated that trace elements contribute in discriminating peridotitic spinels from those crystallized from magmas. Among the elements that are not correlated with Cr# or Mg# content, Zn and Co seem to be the most interesting well separating peridotitic from magmatic occurrences.

Acknowledgements

The Italian C.N.R. financed the installation and maintenance of the electron microprobe laboratory in Padova. L. Furlan, R. Carampin and L. Tauro are kindly acknowledged for technical support. Aka F. Tongwa and Enzo M. Piccirillo contributed to the sampling in Cameroon. DL would like to thank the PRIN 2010-11 fund (SPIN GEO TECH; Responsible FP) and FRA2013 Trieste University fund (Mantle xenoliths in Cenozoic magmas from North-Western Africa: structural and chemical study via SC-XRD, LA-ICP-MS, NRA and μ-CT; Responsible DL). JM received support from IDL through PEst-OE/CTE/UI0263/2014. The editorial handling of Nelson Eby and two anonymous referees are kindly acknowledged for their comments and suggestions.

Appendix A. Supplementary data

Supplementary data to this article can be found online at http://dx.doi.org/10.1016/j.lithos.2017.02.012.

References

Abdelsalam, M.G., Gao, S.S., Liégeois, J.-P., 2011. Upper mantle structure of the Saharan Metacraton. Journal of African Earth Sciences 60, 328–336.

Akmaz, R.M., Uysal, I., Saka, S., 2014. Compositional variations of chromite and solid inclusions in ophiolitic chromitites from the southeastern Turkey: implications for chromitite genesis. Ore Geology Reviews 58, 208–224.

Bardintzeff, J.-M., Deniel, C., Guillou, H., Platevoet, B., Télouk, P., Oun, K.M., 2012. Miocene to recent alkaline volcanism between Al Haruj and Waw an Namous (southern Libya). International Journal of Earth Sciences 101, 1047–1063.

Basso, R., Comin-Chiaramonti, P., Della Giusta, A., Flora, O., 1984. Crystal chemistry of four Mg-Fe-Al-Cr spinels from the Balmuccia peridotite (Western Italian Alps). Neues Jahrbuch für Mineralogie Abhlandungen 150, 1–10.

Beccaluva, L., Azzouni-Sekkal, A., Benhallou, A., Bianchini, G., Ellam, R.M., Marzola, M., Siena, F., Stuart, F.M., 2007. Intracratonic asthenosphere upwelling and lithosphere rejuvenation beneath the Hoggar swell (Algeria): evidence from HIMU metasomatised lherzolite mantle xenoliths. Earth and Planetary Science Letters 260, 482–494.

Beccaluva, L., Bianchini, G., Ellam, R.M., Marzola, M., Oun, K.M., Siena, F., Stuart, F.M., 2008. The role of HIMU metasomatic components in the North African lithospheric mantle: petrological evidence from the Gharyan lherzolite xenoliths, NW Libya. In: Coltorti, M., Gregoire, M. (Eds.), Metasomatism in Oceanic and Continental Lithospheric Mantle. Geological Society of London Special Publication vol. 293, pp. 253–277.

Begg, G.C., Griffin, W.L., Natapov, L.M., O'Reilly, S.Y., Grand, S.P., Hronsky, J.M.A., Djomani, Y.P., Swain, C.J., Deen, T., Bowden, P., 2009. The lithospheric architecture of Africa: seismic tomography, mantle petrology, and tectonic evolution. Geosphere 5, 23–50.

Bosi, F., Andreozzi, G.B., Ferrini, V., Lucchesi, S., 2004. Behavior of cation vacancy in kenotetrahedral Cr-spinels from Albanian eastern belt ophiolites. American Mineralogist 89, 1367–1373.

Brizi, E., Nazzareni, S., Principalle, F., Zanazzi, P.F., 2003. Clinopyroxenes from mantlerelated xenocrysts in alkaline basalts from Hannuoba (China): augite–pigeonite exsolutions and their thermal significance. Contributions to Mineralogy and Petrology 145, 578–584.

Busrewil, M.T., Wadsworth, W.J., 1982–1983. The basalts and associated lherzolite xenoliths of Waw-an-Namus Volcano, Libya. Libyan Journal of Science 2, 19–28.

Carbonin, S., Russo, U., Della Giusta, A., 1996. Cation distribution in some natural spinels from X-ray diffraction and Mössbauer spectroscopy. Mineralogical Magazine 60, 355–368.

Carbonin, S., Menegazzo, G., Lenaz, D., Principalle, F., 1999. Crystal chemistry of two detrital Cr-spinels with unusual low values of oxygen positional parameter: oxidation mechanism and possible clues to their origin. Neues Jahrbuch für Mineralogie Monatshefte 359–371.

Carraro, A., 2003. Crystal chemistry of Cr-spinels from a suite of spinel peridotite mantle xenoliths from the Predazzo Area (Dolomites, Northern Italy). European Journal of Mineralogy 15, 681–688.

Chako Tchamabé, B., Youmen, D., Owona, S., Issa Ohba, T., Németh, K., Nsangou Ngapna, M., Asaah, A.N.E., Aka, F.T., Tanyileke, G., Hell, J.V., 2013. Eruptive history of the Barombi Mbo Maar, Cameroon Volcanic Line, Central Africa: constraints from volcanic facies analysis. Central European Journal of Geosciences 5, 480–496.

Chanouan, L., Ikenne, M., Gahlan, H.A., Arai, S., Youbi, N., 2017. Petrological characteristics of mantle xenoliths from the Azrou-Timahdite quaternary basalts, Middle Atlas, Morocco: A mineral chemistry perspective. Journal of African Earth Sciences http://dx.doi.org/10.1016/j.jafrearsci.2016.09.004 (in press).

Colás, V., González-Jiménez, J.M., Griffin, W.L., Fanlo, I., Gervilla, F., O'Reilly, S.Y., Pearson, N.J., Kerestedjian, T., Proenza, J.A., 2014. Fingerprints of metamorphism in chromite: new insights from minor and trace elements. Chemical Geology 389, 137–152.

Cundari, A., Dal Negro, A., Piccirillo, E.M., Della Giusta, A., Secco, L., 1986. Intracrystalline relationships in olivine, orthopyroxene, clinopyroxene and spinel from a suite of spinel lherzolite xenoliths from Mt. Noorat, Victoria, Australia. Contributions to Mineralogy and Petrology 94, 523–532.

Dal Negro, A., Carbonin, S., Domenghetti, C., Molin, G.M., Cundari, A., Piccirillo, E.M., 1984. Crystal chemistry and evolution of the clinopyroxene in a suite of high pressure ultramafic nodules from the Newer Volcanics of Victoria, Australia. Contributions to Mineralogy and Petrology 86, 221–229.

Dal Negro, A., Manoli, S., Secco, L., Piccirillo, E.M., 1989. Megacrystic clinopyroxenes from Victoria (Australia): crystal chemical comparison of clinopyroxenes from high and low pressure regimes. European Journal of Mineralogy 1, 105–121.

Dare, S.A.S., Pearce, J.A., McDonald, I., Styles, M.T., 2009. Tectonic discrimination of peridotites using fO_2–Cr# and Ga–Ti–Fe^{III} systematics in chrome-spinel. Chemical Geology 261, 199–216.

De Plaen, R.S.M., Bastow, I.D., Chambers, E.L., Keir, D., Gallacher, R.J., Keane, J., 2014. The development of magmatism along the Cameroon Volcanic Line: evidence from seismicity and seismic anisotropy. Journal of Geophysical Research: Solid Earth 4233–4252.

Della Giusta, A., Principalle, F., Carbonin, S., 1986. Crystal chemistry of a suite of natural Cr-bearing spinels with 0.15 < Cr < 1.07. Neues Jahrbuch für Mineralogie Abhandlungen 155, 319–330.

Della Giusta, A., Carbonin, S., Ottonello, G., 1996. Temperature-dependent disorder in a natural Mg–Al–Fe^{2+}–Fe^{3+}–spinel. Mineralogical Magazine 60, 603–616.

Derbyshire, E.J., O'Driscoll, B., Lenaz, D., Gertisser, R., Kronz, A., 2013. Compositionally heterogeneous podiform chromitite in the Shetland Ophiolite Complex (Scotland): implications for chromitite petrogenesis and late-stage alteration in the upper mantle portion of a supra-subduction zone ophiolite. Lithos 162-163, 279–300.

Deruelle, B., Ngounouno, I., Demaiffe, D., 2007. The Cameroon Hot Line (CHL): a unique example of active alkaline intraplate structure in both oceanic and continental lithospheres. Comptes Rendus Geoscience 339, 589–600.

Di Rocco, T., Freda, C., Gaeta, M., Mollo, S., Dallai, L., 2012. Magma chambers emplaced in carbonate substrate. Petrogenesis of skarn and cumulate rocks and implications for CO_2 degassing in volcanic areas. Journal of Petrology 53, 2307–2332.

Duggen, S., Hoernle, K., Van Den Bogaard, P., Garbe-Schönbrg, A., 2005. Post-collisional transition from subduction to intraplate-type magmatism in the westernmost Mediterranean: evidence for continental-edge delamination of subcontinental lithosphere. Journal of Petrology 46, 1155–1201.

Duggen, S., Hoernle, K.A., Hauff, F., Klügel, A., Bouabdellah, M., Thirlwall, M.F., 2009. Flow of canary mantle plume material through a subcontinental lithospheric corridor beneath Africa to the Mediterranean. Geology 37, 283–286.

Dunlop, H.M., 1983. Strontium isotope geochemistry and Potassium–Argon studies of volcanic rocks from the Cameroon Line, West Africa. Unpublished Ph.D. Thesis. Univ. Edinburgh, 347 pp.

Eggins, S.M., Kinsley, L.P.J., Shelley, J.M.G., 1998. Deposition and element fractionation processes during atmospheric pressure laser sampling for analysis by ICP-MS. Applied Surface Science 127–129, 278–286.

El Azzouzi, M., Bernard-Griffiths, J., Bellon, H., Maury, R.C., Pique, A., Fourcade, S., Cotten, J., Hernandez, J., 1999. Evolution des sources du volcanisme marocain au cours du Néogène. Comptes Rendus de L'Academie des Sciences 329, 95–102.

El Azzouzi, M., Maury, R.C., Bellon, H., Youbi, N., Cotton, J., Kharbouch, F., 2010. Petrology and K–Ar chronology of the Neogene–Quaternary Middle Atlas basaltic province, Morocco. Bulletin de la Société Géologique de France 181, 243–257.

El Messbahi, H., Bodinier, J.-L., Vauchez, A., Dautria, J.-M., Ouali, H., Garrido, C.J., 2015. Short wavelength lateral variability of lithospheric mantle beneath the Middle Atlas (Morocco) as recorded by mantle xenoliths. Tectonophysics 650, 34–52.

Elsheikh, A.A., Gao, S.S., Liu, K.H., 2014. Formation of the Cameroon Volcanic Line by lithospheric basal erosion: insight from mantle seismic anisotropy. Journal of African Earth Sciences 100, 96–108.

Farahat, E.S., Abdel Ghani, M.S., Aboazom, A.S., Asran, A.M.H., 2006. Mineral chemistry of Al Haruj low-volcanicity rift basalts, Libya: implications for petrogenetic and geotectonic evolution. Journal of African Earth Sciences 45, 198–212.

Fitton, J.D., Dunlop, H.M., 1985. The Cameroon line, West Africa and its bearing on the origin of oceanic and continental alkali basalts. Earth and Planetary Science Letters 72, 23–38.

Freeth, S.J., Rex, D.C., 2000. Constraints on the age of Lake Nyos, Cameroon. Journal of Volcanology and Geothermal Research 97, 261–269.

Frizon De Lamotte, D., Crespo-Blanc, A., Saint-B'Ezar, B., Comas, M., Fernandez, M., Zeyen, H., Ayarza, H., Robert-Charrue, C., Chalouan, A., Zizi, M., Teixell, A., Arboleya, M.L., Alvarez-Lobato, F., Julivert, M., Michard, A., 2004. TRANSMED-transect I: Betics, Alboran Sea, Rif, Moroccan Meseta, High Atlas, Jbel Saghro, Tindouf Basin. In: Cavazza, W., Roure, F., Spakman, W., Stampfli, G.M., Ziegler, P.A. (Eds.), The TRANSMED Atlas — the Mediterranean Region from Crust to Mantle. Springer, Berlin, pp. 91–96.

González-Jiménez, J.M., Augé, T., Gervilla, F., Bailly, L., Proenza, J.A., Griffin, W.L., 2011. Mineralogy and geochemistry of platinum-rich chromitites from the mantle–crust transition zone at Ouen Island, New Caledonia ophiolite. Canadian Mineralogist 49, 1549–1570.

González-Jiménez, J.M., Griffin, W.L., Proenza, J.A., Gervilla, F., O'Reilly, S.Y., Akbulut, M., Pearson, N.J., Arai, S., 2014. Chromitites in ophiolites: how, where, when, why? Part II. The crystallization of chromitites. Lithos 189, 140–158.

González-Jiménez, J.M., Locmelis, M., Belousova, E., Griffini, W.L., Gervilla, F., Kerestedjian, T.N., O'Reilly, S.Y., Pearson, N.J., Sergeeva, I., 2015. Genesis and tectonic implications of podiform chromitites in the metamorphosed ultramafic massif of Dobromirtsi (Bulgaria). Gondwana Research 27, 555–574.

Guiraud, R., 1998. Mesozoic rifting and basin inversion along the northern African Tethyan margin: an overview. Geological Society, London, Special Publications 132, 217–229.

Günther, D., Heinrich, C.A., 1999. Enhanced sensitivity in laser ablation-ICP mass spectrometry using helium-argon mixtures as aerosol carrier. Journal of Analytical Atomic Spectrometry 14, 1363–1368.

Hill, R.J., Craig, J.R., Gibbs, G.V., 1979. Systematics of the spinel structure type. Physics and Chemistry of Minerals 4, 317–339.

Hu, Z., Gao, S., Liu, Y., Hu, S., Chen, H., Yuan, H., 2008. Signal enhancement in laser ablation ICP-MS by addition of nitrogen in the central channel gas. Journal of Analytical Atomic Spectrometry 23, 1093–1101.

Kamenetsky, V., Crawford, A.J., Meffre, S., 2001. Factors controlling chemistry of magmatic spinel: an empirical study of associated olivine, Cr-spinel and melt inclusions from primitive rocks. Journal of Petrology 42, 655–671.

Kourim, F., Bodinier, J.L., Alard, O., Bendaoud, A., Vauchez, A., Dautria, J.M., 2014. Nature and evolution of the lithospheric mantle beneath the Hoggar swell (Algeria): a record from mantle xenoliths. Journal of Petrology 55, 2249–2280.

Lasserre, M., 1978. Mise au point Sur les granitoıdes dits "ultimes" du Cameroun. Gisements petrographie et geochronologie. Bulletin Bureau Recherches Geologiques Minieres. Section 4: Geologie Generale 2, 143–159.

Lavina, B., Salviulo, G., Della Giusta, A., 2002. Cation distribution and structure modeling of spinel solid solutions. Physics and Chemistry of Minerals 29, 10–18.

Lenaz, D., Kamenetsky, V.S., Crawford, A.J., Principalle, F., 2000. Melt inclusions in detrital spinels from the SE Alps (Italy–Slovenia): a new approach to provenance studies of sedimentary basins. Contributions to Mineralogy and Petrology 139, 748–758.

Lenaz, D., Andreozzi, G.B., Mitra, S., Bidyananda, M., Principalle, F., 2004. Crystal chemical and ^{57}Fe Mössbauer study of chromite from the Nuggihalli schist belt (India). Mineralogy and Petrology 80, 45–57.

Lenaz, D., Braidotti, R., Principalle, F., Garuti, G., Zaccarini, F., 2007. Crystal chemistry and structural refinement of chromites from different chromitite layers and xenoliths of the Bushveld Complex. European Journal of Mineralogy 19, 599–609.

Lenaz, D., Logvinova, A.M., Principalle, F., Sobolev, N.V., 2009. Structural parameters of chromite included in diamonds and kimberlites from Siberia: a new tool for discriminating ultramafic source. American Mineralogist 94, 1067–1070.

Lenaz, D., De Min, A., Garuti, G., Zaccarini, F., Principalle, F., 2010. Crystal chemistry of Cr-spinels from the lherzolite mantle peridotite of Ronda (Spain). American Mineralogist 95, 1323–1328.

Lenaz, D., O'Driscoll, B., Principalle, F., 2011. Petrogenesis of the anorthosite-chromitite association: crystal-chemical and petrological insights from the Rum Layered Suite, NW Scotland. Contributions to Mineralogy and Petrology 162, 1201–1213.

Lenaz, D., Garuti, G., Zaccarini, F., Cooper, R.W., Principalle, F., 2012. The Stillwater Complex chromitites: the response of chromite crystal chemistry to magma injection. Geologica Acta 10, 33–41.

Lenaz, D., Skogby, H., Logvinova, A.M., Sobolev, N.V., Principalle, F., 2013. A micro-Mössbauer study of chromites included in diamond and other mantle-related rocks. Physics and Chemistry of Minerals 40, 461–479.

Lenaz, D., Youbi, N., De Min, A., Boumehdi, M.A., Ben Abbou, M., 2014a. Low intra-crystalline closure temperatures of Cr-bearing spinels from the mantle xenoliths of the Middle Atlas Neogene-Quaternary Volcanic Field (Morocco): a mineralogical evidence of a cooler mantle beneath the West African Craton. American Mineralogist 99, 267–275.

Lenaz, D., Adetunji, J., Rollinson, H., 2014b. Determination of $Fe^{3+}/\Sigma Fe$ ratios in chrome spinels using a combined Mössbauer and single-crystal X-ray approach: application to chromitites from the mantle section of the Oman ophiolite. Contributions to Mineralogy and Petrology 167, 958.

Lenaz, D., Andreozzi, G.B., Bidyananda, M., Principalle, F., 2014c. Oxidation degree of chromite from Indian ophiolites: a crystal chemical and ^{57}Fe Mössbauer study. Periodico di Mineralogia 83, 241–255.

Lenaz, D., Princivalle, F., Schmitz, B., 2015. First crystal-structure determination of chromites from an acapulcoite and ordinary chondrites. Mineralogical Magazine 79, 755–765.
Lucchesi, S., Bosi, F., Pozzuoli, A., 2010. Geothermometric study of Mg-rich spinels from the Somma–Vesuvius volcanic complex (Naples, Italy). American Mineralogist 95, 617–621.
Lustrino, M., Wilson, M., 2007. The circum Mediterranean anorogenic Cenezoic igneous province. Earth Science Reviews 81, 1–65.
Martin, U., Németh, K., 2006. How strombolian is a "Strombolian"scoria cone? Some irregularities in scoria cone architecture from the Transmexican Volcanic Belt, near Volcán Ceboruco, (Mexico) and Al Haruj (Libya). Journal of Volcanology and Geothermal Research 155, 104–118.
Marzoli, A., Piccirillo, E.M., Renne, P.R., Bellieni, G., Iacumin, M., Nyobe, J.B., Tongwa, A.T., 2000. The Cameroon Volcanic line revisited: petrogenesis of continental basaltic magmas from lithospheric and asthenospheric mantle sources. Journal of Petrology 42, 197–218.
Marzoli, A., Aka, F.T., Merle, R., Callegaro, S., N'ni, J., 2015. Deep to shallow crustal differentiation of within-plate alkaline magmatism at Mt. Bambouto volcano, Cameroon line. Lithos 220-223, 272–288.
Maury, R.C., Fourcade, S., Coulon, C., El Azzouzi, M., Bellon, H., Coutelle, A., Ouabadi, A., Semroud, B., Megartsi, M., Cotton, J., Belanteur, O., Lounni-Hacini, A., Piqué, A., Capdevila, R., Hernandez, J., Rehault, J.-P., 2000. Post-collisional Neogene magmatism of the Mediterranean Maghreb margin: a consequence of slab breakoff. Comptes Rendus de l'Academie des Sciences Paris, II 331 (3), 159–173 (série II).
McGowan, N., Griffin, W.L., Gonzalez-Jimenez, J.M., Belousova, E.A., Afonso, J.C., Shi, R., McCammon, C., Pearson, N.J., O'Reilly, S.Y., 2015. Tibetan chromitites: excavating the slab graveyard. Geology 43, 179–182.
Miller, C., Zanetti, A., Thöni, M., Konzett, J., Klötzli, U., 2012. Mafic and silica-rich glasses in mantle xenoliths from Wau-En-Namus, Libya: textural and geochemical evidence for peridotite-melt reactions. Lithos 128-131, 11–26.
Missenard, Y., Zeyen, H., Frizon de Lamotte, D., Leturmy, P., Petit, C., Sebrier, M., Saddiqi, O., 2006. Crustal versus asthenospheric origin of relief of the Atlas Mountains of Morocco. Journal of Geophysical Research 111:B03401. http://dx.doi.org/10.129/2005JB003708.
Natali, C., Beccaluva, L., Bianchini, G., Ellam, R.M., Siena, F., Stuart, F.M., 2013. Carbonated alkali-silicate metasomatism in the North Africa lithosphere: evidence from Middle Atlas spinel–lherzolites, Morocco. Journal of South American Earth Sciences 41, 113–121.
Nédli, Zs, Princivalle, F., Lenaz, D., Tóth, T.M., 2008. Crystal chemistry of clinopyroxene and spinel from mantle xenoliths hosted in Late Mesozoic lamprophyres (Villány Mts, S Hungary). Neues Jahrbuch für Mineralogie Abhandlungen 185, 1–10.
Nédli, Zs, Princivalle, F., Dobosi, G., Embey-Isztin, A., 2009. Crystal chemistry of clinopyroxenes from upper-mantle xenolith series in the Balaton–Bakony volcanic area (Carpathian–Pannonian region, Hungary). European Journal of Mineralogy 21, 433–442.
Németh, K., Suwesi, K.S., Peregi, Z., Gulácsi, Z., Ujszászi, J., 2003. Plio/Pleistocene flood basalt related scoria and spatter cones, rootless lava flows, and pit craters, Al Haruj Al Abiyad, Libya, Geolines. Journal of the Geological Institute AS Czech Republic 15, 98–103.
Ngako, V., Njonfang, E., Aka, F.T., Affaton, P., Nnange, J.M., 2006. The north–south Paleozoic to Quaternary trend of alkaline magmatism from Niger–Nigeria to Cameroon: complex interaction between hotspots and Precambrian faults. Journal of African Earth Sciences 45, 241–256.
Nkono, C., Féménias, O., Demaiffe, D., 2014. Geodynamical model for the development of the Cameroon Hot Line (Equatorial Africa). Journal of African Earth Sciences 100, 626–633.
Nkouandou, O.F., Bardintzeff, J.M., Fagny, A.M., 2015. Sub-continental lithospheric mantle structure beneath the Adamawa plateau inferred from the petrology of ultramafic xenoliths from Ngaoundéré (Adamawa plateau, Cameroon, Central Africa). Journal of African Earth Sciences 111, 26–40.
Nyome, M.S., de Wit, M.J., 2014. The Cameroon line: analyses of an intraplate magmatic province transecting both oceanic and continental lithospheres: constraints, controversies and models. Earth-Science Reviews 139, 168–194.
O'Reilly, S.Y., Zhang, M., Griffin, W.L., Begg, G., Hronsky, J., 2009. Ultradeep continental roots and their oceanic remnants: a solution to the geochemical "mantle reservoir" problem? Lithos 211S, 1043–1054.
Pagé, P., Barnes, S.-J., 2009. Using trace elements in chromites to constrain the origin of podiform chromitites in the Thetford Mines ophiolite, Québec, Canada. Economic Geology 104, 997–1018.
Pearce, J.G.N., Perkins, W.T., Westgate, J.A., Gorton, M.P., Jackson, S.E., Neal, C.R., Chenery, S.P., 1997. A compilation of new and published major and trace element data for NIST SRM 610 and NIST SRM 612 glass reference materials. Geostandards Newsletter 21, 115–144.
Perinelli, C., Bosi, F., Andreozzi, G.B., Conte, A.M., Armienti, P., 2014. Geothermometric study of Cr-spinels of peridotite mantle xenoliths from Northern Victoria Land (Antarctica). American Mineralogist 99, 839–846.
Permenter, J.L., Oppenheimer, C., 2007. Volcanoes of the Tibesti massif (Chad, northern Africa). Bulletin of Volcanology 69, 609–626.
Petrelli, M., Morgavi, D., Vetere, F., Perugini, D., 2016. Elemental imaging and petro-volcanological applications of an improved Laser Ablation Inductively Coupled Quadrupole Plasma Mass Spectrometry. Periodico di Mineralogia 85, 25–39.
Pintér, Z., Patkó, L., Tene Djoukam, J.F., Kovács, I., Tchouankoue, J.P., Falus, G., Konc, Z., Tommasi, A., Barou, F., Mihály, J., Németh, C., Jeffries, T., 2015. Characterization of the sub-continental lithospheric mantle beneath the Cameroooon Volcanic Line inferred from alkaline basalt hosted peridotite xenoliths from Barombi Mbo and Nyos Lakes. Journal of African Earth Sciences 111, 170–193.
Prince, E., 2004. International Tables for X-ray Crystallography. Volume C: Mathematical, Physical and Chemical Tables. 3rd ed. Springer, Dordrecht, The Netherlands.
Princivalle, F., Della Giusta, A., Carbonin, S., 1989. Comparative crystal chemistry of spinels from some suites of ultramafic rocks. Mineralogy and Petrology 40, 117–126.
Princivalle, F., Della Giusta, A., De Min, A., Piccirillo, E.M., 1999. Crystal chemistry and significance of cation ordering in Mg–Al rich spinels from high-grade hornfels (Predazzo-Monzoni, NE Italy). Mineralogical Magazine 63, 257–262.
Princivalle, F., Salviulo, G., Marzoli, A., Piccirillo, E.M., 2000. Clinopyroxene of spinel peridotite mantle xenoliths from Lake Nji (Cameroon Volcanic Line, W Africa): crystal chemistry and petrological implications. Contributions to Mineralogy and Petrology 139, 503–508.
Princivalle, F., De Min, A., Lenaz, D., Scarbolo, M., Zanetti, A., 2014. Ultramafic xenoliths from Damaping (Hannuoba region, NE-China): petrogenetic implications from crystal chemistry of pyroxenes, olivine and Cr-spinel and trace element content of clinopyroxene. Lithos 188, 3–14.
Raffone, N., Chazot, G., Pin, C., Vannucci, R., Zanetti, A., 2009. Metasomatism in the lithospheric mantle beneath Middle Atlas (Morocco) and the origin of Fe- and Mg-rich wehrlites. Journal of Petrology 50, 197–249.
Reusch, A.M., Nyblade, A.A., Wiens, D.A., Shore, P.J., Ateba, B., Tabod, C.T., Nnange, J.M., 2010. Upper mantle structure beneath Cameroon from body wave tomography and the origin of the Cameroon Volcanic Line. Geochemistry, Geophysics, Geosystems 11, Q10W07.
Reusch, A.M., Nyblade, A.A., Tibi, R., Wiens, D., Shore, P., Bekoa, A., Tabod, C.T., Nnange, J.M., 2011. Mantle transition zone thickness beneath Cameroon: evidence for an upper mantle origin for the Cameroon Volcanic Line. Geophysical Journal International 187, 1146–1150.
Rocholl, A., 1998. Major and trace element composition and homogeneity of microbeam reference material: basalt glass USGS BCR-2G. Geostandards Newsletter 22, 33–45.
Sheldrick, G.M., 2008. A short history of SHELX. Acta Crystallographica A64, 112–122.
Tamen, J., Nkoumbou, C., Mouafo, L., Reusser, E., Tchoua, F.M., 2007. Petrology and geochemistry of monogenetic volcanoes of the Barombi Koto volcanic field (Kumba Graben, Cameroon volcanic line): implications for mantle source characteristics. Comptes Rendus Géosciences 339, 799–809.
Tchouankoue, J.P., Simeni Wambo, N.A., Dongmo, A.K., Li, X.-H., 2014. $^{40}Ar/^{39}Ar$ dating of basaltic dykes swarm in Western Cameroon: evidence of Late Paleozoic and Mesozoic magmatism in the corridor of the Cameroon Line. Journal of African Earth Sciences 93, 14–22.
Teitchou, M.I., Grégoire, M., Dantas, C., Tchoua, F.M., 2007. High mantle beneath the Kumba plain (Cameroon line), after spinel peridotite xenolith in basaltic lava. Comptes Rendus Geoscience 33, 101–109.
Teixell, A., Ayarza, P., Zeyen, H., Fernandez, M., Arboleya, M.-L., 2005. Effects of mantle upwelling in a compressional setting: the Atlas Mountains of Morocco. Terra Nova 17, 456–461.
Temdjim, R., 2005. Contribution à la connaissance du manteau supérieur du Cameroun au travers de l'étude des enclaves ultrabasiques et basiques remontées par les volcans de Youkou (Adamaoua) et de Nyos (ligne du Cameroun). (Thèse Doct d'Etat). Uni Yaoundé (418 pp.).
Temdjim, R., 2012. Ultramafic xenoliths from Lake Nyos area, Cameroon volcanic line, West-central Africa: petrography, mineral chemistry, equilibration conditions and metasomatic features. Chemie der Erde 72, 39–60.
Tokonami, M., 1965. Atomic scattering factor for O^{-2}. Acta Crystallographica 19, 486.
Trompette, R., 1994. In: Trompette, R., Carozzi, A.V. (Eds.), Geology of Western Gondwana (2000–500 Ma): Pan-African Brasiliano Aggregation of South America and Africa. 364. A.A. Balkema, Rotterdam.
Uchida, H., Lavina, B., Downes, R.T., Chesley, J., 2005. Single-crystal X-ray diffraction of spinels from the San Carlos Volcanic Field, Arizona: spinel as a geothermometer. American Mineralogist 90, 1900–1908.
Velicogna, M., Lenaz, D., 2017. Is 600°C enough to produce air oxidation in Cr-spinels? Neues Jahrbuch für Mineralogie Abhandlungen (in print).
Wittig, N., Pearson, D.G., Baker, J.A., Duggen, S., Hoernle, K., 2010a. A major element, PGE and Re–Os isotope study of Middle Atlas (Morocco) peridotite xenoliths: evidence for coupled introduction of metasomatic sulphides and clinopyroxene. Lithos 115, 15–26.
Wittig, N., Pearson, D.G., Duggen, S., Baker, J.A., Hoernle, K., 2010b. Tracing the metasomatic and magmatic evolution of continental mantle roots with Sr, Nd, Hf and Pb isotopes: a case study of Middle Atlas (Morocco) peridotite xenoliths. Geochimica et Cosmochimica Acta 74, 1417–1435.
Woller, F., Fediuk, F., 1980. Volcanic rocks of Jabal as Sawda. In: Salem, M.J., Busrewil, M.T. (Eds.), The Geology of Libya. vol. III. Academic Press, London, pp. 1081–1093.
Zeyen, H., Ayarza, P., Fernandez, M., Rimi, A., 2005. Lithospheric structure under the western African–European plate boundary: a transect across the Atlas Mountains and the Gulf of Cadiz. Tectonics 24:1–16, TC2001. http://dx.doi.org/10.129/2004TC001639.
Zhou, M.-F., Robinson, P.T., Su, B.-X., Gao, J.-F., Li, J.-W., Yang, J.-S., Malpas, J., 2014. Compositions of chromite, associated minerals, and parental magmas of podiform chromite deposits: the role of slab contamination of asthenospheric melts in suprasubduction zone environments. Gondwana Research 26, 262–283.
Ziberna, L., Nimis, P., Zanetti, A., Marzoli, A., Sobolev, N., 2013. Metasomatic processes in the Central Siberian cratonic mantle: evidence from garnet xenocrysts from the Zagadochnaya kimberlite. Journal of Petrology 54, 2379–2409.